EJN European Journal of Neuroscience

FENS Federation of European Neuroscience Societies

European Journal of Neuroscience, Vol. 42, pp. 2390–2406, 2015 doi:10.1111/ejn.13019

NEUROSYSTEMS

Context-dependent coding and gain control in the auditory system of crickets

Jan Clemens,[1,2,3] Florian Rau,[1] R. Matthias Hennig[1] and K. Jannis Hildebrandt[4,5]
[1]Behavioral Physiology Group, Department of Biology, Humboldt-Universität zu Berlin, Berlin, Germany
[2]Bernstein Center for Computational Neuroscience Berlin, Berlin, Germany
[3]Princeton Neuroscience Institute, Princeton University, Washington Road, Princeton, NJ 08540, USA
[4]Cluster of Excellence 'Hearing4all', Department for Neuroscience, University of Oldenburg, Oldenburg, Germany
[5]Research Center Neurosensory Science, University of Oldenburg, Oldenburg, Germany

Keywords: adaptive coding, auditory coding, cricket, gain control, inhibition

Abstract

Sensory systems process stimuli that greatly vary in intensity and complexity. To maintain efficient information transmission, neural systems need to adjust their properties to these different sensory contexts, yielding adaptive or stimulus-dependent codes. Here, we demonstrated adaptive spectrotemporal tuning in a small neural network, i.e. the peripheral auditory system of the cricket. We found that tuning of cricket auditory neurons was sharper for complex multi-band than for simple single-band stimuli. Information theoretical considerations revealed that this sharpening improved information transmission by separating the neural representations of individual stimulus components. A network model inspired by the structure of the cricket auditory system suggested two putative mechanisms underlying this adaptive tuning: a saturating peripheral nonlinearity could change the spectral tuning, whereas broad feed-forward inhibition was able to reproduce the observed adaptive sharpening of temporal tuning. Our study revealed a surprisingly dynamic code usually found in more complex nervous systems and suggested that stimulus-dependent codes could be implemented using common neural computations.

Introduction

One of the most challenging tasks for sensory systems is to identify signals from separate sources in complex, natural environments. If neuronal filters are too wide, coding is unselective and multiple co-occurring signals can mask and distort important information (Narayan *et al.*, 2007). However, integration with wide filters can enhance sensitivity for weak signals or help to reduce noise (Pouget *et al.*, 1999; Zhang & Sejnowski, 1999).

Thus, from the perspective of sensory coding, there is a trade-off between the integration of information across the whole bandwidth of a given signal and more selective coding of dominant elements to reduce potential interference (Seriès *et al.*, 2004). Ideally, the balance between separation and integration should be adjusted to the current sensory environment in order to make efficient use of available information. The trade-off between selectivity and sensitivity is often solved by adapting neuronal tuning to the stimulus statistics and yields context-dependent and stimulus-dependent codes (Vinje & Gallant, 2000; Machens *et al.*, 2004; Borst *et al.*, 2005; Chacron *et al.*, 2005; Ahrens *et al.*, 2008; Schneider & Woolley, 2011; Massot *et al.*, 2012). Context-dependent codes thus optimise coding by either exploitation of valuable context information in nonlinear combinatorial codes [e.g. responses to bird's own song (Margoliash & Konishi, 1985)] or suppression of background noise (Sobel & Tank, 1994). The main mechanisms underlying the emergence of these adaptive codes are inhibition and peripheral nonlinearities (Carandini & Heeger, 2012).

Although context-dependent coding has been studied in complex neural systems, we investigate here whether a small model system with only three major cell types and well-defined tasks (the peripheral auditory system of the cricket) exhibits equally complex codes. Crickets encode and process sound in two behaviorally relevant frequency channels (Nolen & Hoy, 1984; Pollack & Imaizumi, 1999). Low carrier frequencies are associated with mating signals and elicit approaching behavior; high carrier frequencies induce avoidance behavior as they are associated with the echolocation signals of cricket-hunting bats (Wyttenbach *et al.*, 1996; Marsat & Pollack, 2006). Sound is encoded by three main interneurons of the prothoracic ganglion (Pollack & Imaizumi, 1999): ascending neuron (AN)1, AN2, and the omega neuron 1 (ON1). All three of these neurons receive direct receptor input (Hennig, 1988; Pollack, 1994). Whereas ON1 is tuned to a broad range of carrier frequencies, the ANs separate information about low-frequency, conspecific stimuli (AN1) and high-frequency, 'predator' signals (AN2) (Nolen & Hoy, 1984). Despite this separation of the two frequency ranges in AN1 and AN2, there are several sources of potential cross-talk between channels in receptor neurons (Pollack & Imaizumi, 1999; Hennig *et al.*, 2004) and synaptic integration in downstream neurons (Pollack, 1994).

Using recordings from these three cell types, we demonstrate context-dependent coding in the cricket. Linear–nonlinear (LN) models show that spectrotemporal tuning in AN1 and AN2 sharpens

Correspondence: J. Clemens, [3]Princeton Neuroscience Institute, as above.
E-mail: clemensjan@gmail.com

Received 23 June 2014, revised 7 July 2015, accepted 8 July 2015

adaptively when switching from simple to more complex, multi-band stimuli. Information theory demonstrates that this adaptive code reduces interference in the coding of predator and mating signals. Using a model, we propose that this complex code can be implemented in a static network with two mechanisms found in many sensory pathways, i.e. a saturating input nonlinearity in the periphery and broadly-tuned, feed-forward inhibition.

Materials and methods

Electrophysiology

Animals

Adult female *Gryllus bimaculatus* were obtained from a commercial supplier and kept isolated from males. After visually inspecting the intactness of the tympana, the mid and hind legs as well as the wings were removed and the animal was dorsally fixed to the recording stage with wax. The front legs were mounted in a natural position and care was taken not to restrain the tympana with wax. In order to reduce upstream neuronal activity and body movements, both the mesothoracic and metathoracic ganglion were removed. The maxillae, labrum and gut were also removed.

Recordings

Signals from AN1 and AN2 were recorded differentially from one of the connectives between the prothoracic and subesophageal ganglion using tungsten hook electrodes, referenced to a silver wire in the animal's abdomen (Hennig, 1988). Signals from ON1 were recorded in separate sessions from the prothoracic ganglion using an extracellular tungsten electrode (World Precision Instruments, Sarasota, FL, USA), referenced to a stabilising metal spoon.

Voltage signals were band-pass filtered between 300 and 3000 Hz (DPA-2FX; npi electronics, Tamm, Germany), digitised at 20 kHz sampling rate (PCI-6229; National Instruments, Austin, TX, USA) and recorded using LabView software (National Instruments).

After digital-to-analog conversion, audio stimuli were adjusted to the desired sound pressure level (SPL) with an attenuator (ATN-01M; npi electronics), amplified with a power amplifier (Raveland XA-600; Blaupunkt, Hildesheim, Germany) and presented via one of two loudspeakers mounted on either side of the animal. The sound intensity was calibrated to decibels re 2 μPa with a ½-inch condenser microphone (Type 4133, Brüel & Kjær).

Spike sorting

Action potentials were detected by a threshold in the differentiated voltage traces. If the signal-to-noise ratio of the recording allowed it, both ANs were detected in the same voltage trace and sorted by the amplitude of their spikes as AN1 had smaller amplitude spikes than AN2 (Hennig, 1988) (Fig. 1b). Note that spikes of AN2 could potentially mask those of AN1, which would be most detrimental for high frequencies at which AN2 fires most strongly. However, AN1 exhibits a higher latency than AN2 (Hennig, 1988), reducing the probability of missing AN1 spikes coincident with those in AN2. We ensured the identity of the recorded cells by their physiological characteristics (frequency tuning, maximal firing rates, sensitivity to contralateral input). Our data set consisted of five specimens of ON1, six AN1 and 14 AN2.

The neuronal responses were relatively similar across individuals, consistent with previous reports on response stereotypy in these cells (Hennig, 1988). This is corroborated by the small error bars in most figures.

Stimuli

The stimuli consisted of pure tones with a frequency of 4.5, 10, 15, or 25 kHz. The amplitude of the pure tone carriers was randomly modulated by Gaussian low-pass noise with a cut-off of 200 Hz, a mean $\mu = 80$ dB SPL and a SD $\sigma = 6$ dB SPL. These four tones span the range of behaviorally relevant carrier frequencies: 4.5 kHz corresponds to the carrier frequency of the male calling song and can elicit approaching behavior; 15 and 25 kHz are associated with the echolocation signals of bats and elicit escape behavior (Popov & Shuvalov, 1977); and 10 kHz is intermediate between these two frequency ranges and is the dominant frequency in male courtship song (Libersat *et al.*, 1994). The mean and SD were chosen as they fall within the range of naturally occurring intensities and as natural stimuli with these values elicit behavioral responses (Marsat & Pollack, 2006).

The envelope at carrier frequency f is constructed to be Gaussian on a logarithmic decibel scale

$$e_f^{dB}(t) = \mu + \sigma N_f(t)$$

where $N_f(t)$ is zero-mean, unit-variance Gaussian noise. The envelope was exponentiated to a linear voltage signal

$$e_f^{p}(t) = 10^{(\mu + \sigma N_f(t))/20}$$

and multiplied by a sinusoidal carrier $c_f(t)$ of frequency f. These carrier frequencies were represented either individually ('single-band') or as a sum ('multi-band')

$$s(t) = \sum_f c_f(t) e_f^{p}(t)$$

Note that, in the multi-band case, the amplitude of each one of the four carriers was modulated with independent noise; different frequency bands thus had uncorrelated amplitude modulation (AM) patterns.

To estimate the LN models, we presented 20 different stimuli, each of which lasted 20 s. The time-varying firing rate for evaluating the models and computing information was estimated from 20–40 repetitions of the same 4 s stimulus. As all three neurons adapted, we used only the stationary part of the response, by omitting the first 0.4 s of each spike train.

Estimation of linear–nonlinear models

We estimated LN models from the responses to the amplitude-modulated stimuli. Such models consist of two elements: a linear filter that describes a cell's selectivity for (spectro)temporal features of the stimulus and an input–output function (nonlinearity) that relates the filter's output to the cell's firing rate and depicts the tuning of the cell for the filter (Clemens *et al.*, 2012).

Filters were estimated as spike-triggered averages. To that end, the AM in each single band was down-sampled to 1000 Hz and the average envelope in the 64 ms preceding a spike was calculated. Doing this for all four carrier frequencies yielded a set of four filters. For the multi-band stimulus, consisting of four independently amplitude-modulated frequency bands, the spike-triggered average was calculated for each carrier frequency separately, yielding

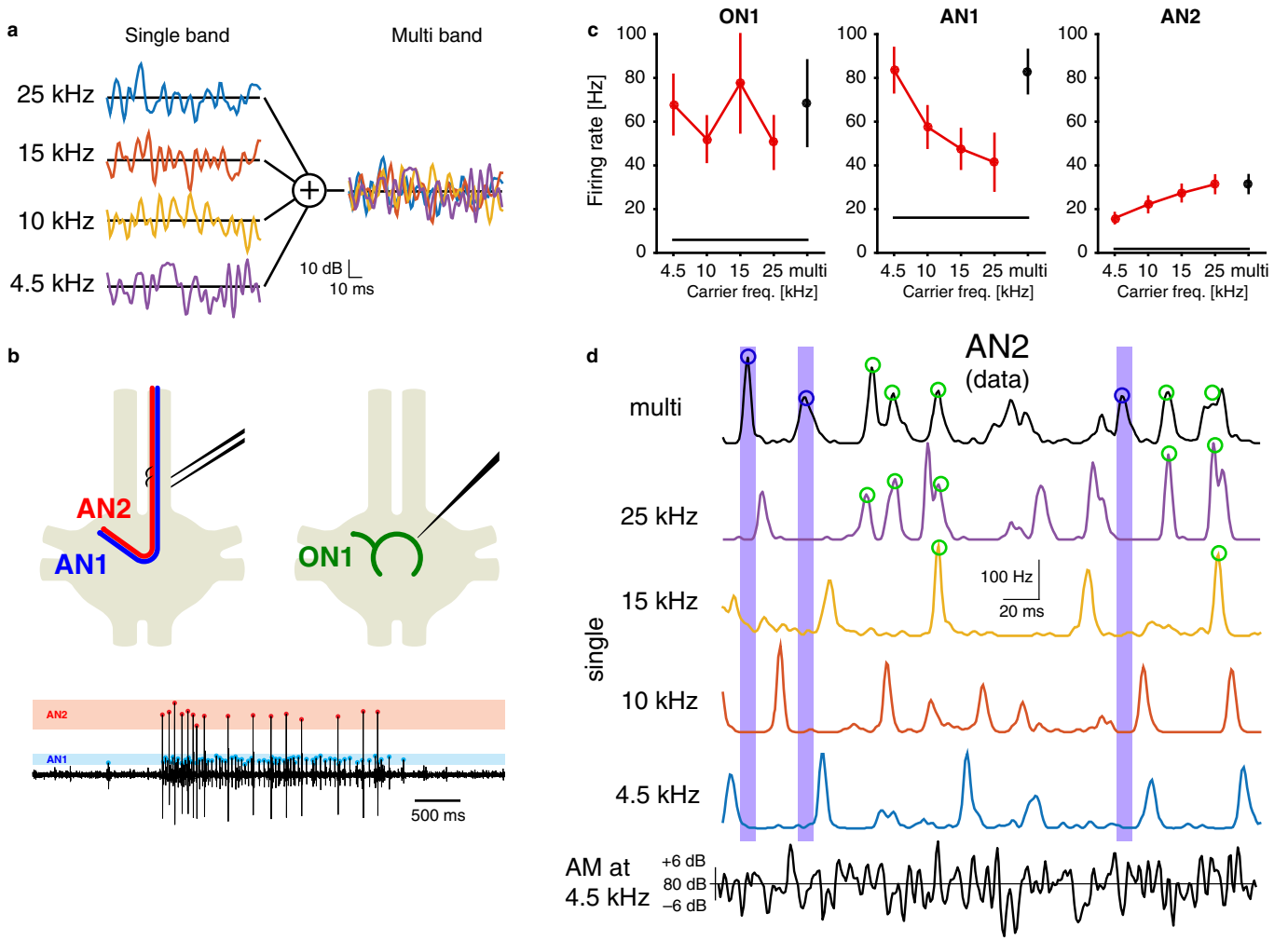

FIG. 1. Data. Coding properties in cricket auditory neurons differ between single-band and multi-band stimuli. (a) We recorded neuronal responses to stimuli with a single carrier frequency ('single band', left) and to the sum of these four single-band stimuli ('multi band', right). Shown is the pattern of random AMs for each frequency band. (b) Spiking responses of the three major neurons in the cricket's early auditory system were recorded extracellularly. AN1 and AN2 were recorded simultaneously from the neck connective (left) and identified by their spike amplitude (bottom). The local neuron ON1 was recorded extracellularly from the prothoracic ganglion (right). (c) Firing rate tuning for the three major neurons in the cricket's early auditory system (ON1, AN1 and AN2). Shown is the mean ± SEM firing rate for the single-band and multi-band stimuli over specimens (red and black, respectively). Average baseline firing rate is shown as a horizontal black line. All three cells responded well to all carrier frequencies. (d) Responses of AN2 to stimuli with different carrier-frequency compositions. Bottom black trace shows the AM pattern for 4.5 kHz. Colored traces depict firing rate for individual single-band stimuli [see (a), left]. Top black trace indicates response to the sum of the four single-band stimuli [see (a), right]. Green circles indicate firing events for the multi-band stimulus that were also present in the single-band stimuli. Pink shading indicates firing events in the multi-band stimuli not associated with a firing event in any single-band response.

another set of four filters. This corresponds to a low-resolution spectrotemporal receptive field, used to analyse the joint tuning of cells for spectral and temporal features of a stimulus (see, e.g. Aertsen & Johannesma, 1981; Atencio *et al.*, 2008).

Model performance was quantified with a novel stimulus not used for the estimation of the filters and input–output functions. The time-varying firing rate of the neuron was estimated from multiple representations of a short noise segment. The spike trains were binned with a resolution of 1 ms and the resulting time-varying firing rate was smoothed with a box window spanning two bins. To predict the response, the stimulus envelope was down-sampled to 1000 Hz and fed into the LN model. A bias-corrected coefficient of correlation between the actual and predicted response served as a measure of model performance (Clemens *et al.*, 2012).

The distance d between filters for single-band and multi-band stimuli was calculated as 1 minus the dot product between normalised filters for each cell type and carrier frequency: $d(f_1,f_2) = 1 - f_1^T f_2$, where f_i are the unit-norm filters as column vectors and ^{T} is the transpose operator.

Encoding model and coherence information

We employed a normative approach to gain insight into how neuronal systems should adapt their properties for different stimulus conditions (single-band vs. multi-band input). The model encoder received uncorrelated Gaussian input on two channels; the encoder filtered and thresholded the stimulus in both channels, and then both inputs were pooled to yield the output firing rate of the cell. This resembles a simplified version of our experimental stimulus paradigm with only two instead of four frequency bands. Filters were taken from the experimental data for AN2 (multi-band stimulus, biphasic filter at 4.5 kHz and low-pass filter at 25 kHz; see Fig. 4a, black filters in bottom row). We examined the impact of adaptive tuning by calculating the information about the envelope pattern for each

individual input for different filter shapes and filter magnitudes. As the input–output function was fixed with a slope of 1 Hz/dB, reducing the filter's scale is equivalent to reducing the cell's output gain.

Coherence information estimates the information retrievable from the neuronal response by optimal linear stimulus reconstruction and yields a lower bound on the mutual information between stimulus and response (Borst & Theunissen, 1999). It is given by $I(f) = -\log_2 (1-C_{sr}(f))$. Stimulus–response coherence is defined as $C_{sr}(f) = |P_{sr}(f)|^2/P_{ss}(f)/P_{rr}(f)$, where P_{sr} is the cross-spectral density of the stimulus envelope s and the response r, and P_{ss} and P_{rr} are the respective autospectral densities. The total information was obtained by integrating $I(f)$ between 0 and 200 Hz and summing the information for both inputs. The calculation of information in the cell's experimental responses was based on the time-varying firing rates used for model evaluation.

Note that the information rates obtained in this study differ from those observed from homologous neurons in another species of crickets (Marsat & Pollack, 2004, 2005), probably due to cross-species differences. We focus on changes of information with stimulus type and not on the absolute amount of information transmitted by the system.

Network model

We built a minimal network model inspired by the auditory system of the cricket to examine how stimulus-dependent coding can be implemented. Our minimal circuit consisted of two receptor populations (low-frequency and high-frequency), the inhibitory interneuron ON1, and AN1 and AN2. The stimulus envelope was provided by four input channels corresponding to the four carrier frequencies (Fig. 6a). Frequency tuning of the receptor populations was modeled by frequency-specific attenuation (Fig. 6b): input to low-frequency receptors was attenuated most strongly at 15 and 25 kHz (attenuation values: 4.5 kHz, 0 dB; 10 kHz, −8 dB; 15 and 25 kHz, −16 dB); and effective input to high-frequency receptors was weakest at 4.5 kHz (attenuation values: 4.5 kHz, −16 dB; 10 kHz, −8 dB; 15 and 25 kHz, 0 dB) (Imaizumi & Pollack, 1999). This was implemented as a gain factor w_f, with which each carrier frequency was multiplied on the pressure scale (Gollisch *et al.*, 2002). To pool different spectral inputs, we summed the gain-weighted envelope of each carrier frequency on the pressure scale. We then transformed this pooled input to the decibel scale (Fig. 6c). The receptors' firing rate was taken to be linearly proportional to this pooled decibel input: $r(t) \propto \log_{10}\left(\sum_f w_f e_f^p(t)\right)$. For single-band stimuli this reduces to $r(t) \propto \log_{10}\left(e_f^p(t)\right) + \log_{10}(w_f) = 20e_f^d(t) - a_f$. In this case, the multiplicative gain on the pressure scale is subtractive on the decibel scale and therefore does not change the variance or receptor response. To match the time scale of response in the model with those seen in the experimental data, we applied a low-pass filter to each driving receptor response (Gaussian with a SD of 7 ms).

The synapses were modeled with a weight w_{ij} and a delay δ_{ij}. The time-varying firing rate of each of the three neurons in the network was thus the weighted and delayed sum of its inputs (Fig. 6d): $r_i(t) = \sum_j w_{ij} r_j(t - \delta_{ij})$ (inputs j: low-frequency and high-frequency receptors, ON1; outputs i: ON1, AN1, AN2). A list of parameters (synaptic weights w_{ij} and delays ∂_{ij}) can be found in Table 1.

We employed a threshold linear input–output function (threshold 0 Hz, slope 1) to ensure strictly positive firing rates. Note that adding this nonlinearity did not change the properties of the network as the modeled firing rates were rarely below zero.

TABLE 1. List of parameters for the network model

Synapse	Synaptic delay [ms]	Synaptic weight
LF to ON1	10	0.4
HF to ON1	6	0.4
LF to AN1	12	0.3
LF to AN2	12	0.1
HF to AN2	10	0.6
ON1 to AN1	6	−0.15
ON1 to AN2	5	−0.35

LF, low-frequency receptors; HF, high-frequency receptors.

To analyse the encoding properties of the cells in the model, we employed the same framework of LN models as in the analysis of the experimental data.

If possible, network parameters were taken or estimated from the literature (see references below). As no data were available for some parameters (synaptic weights, some synaptic delays), these parameters were chosen based on general biophysical assumptions. Note that none of the results of this study critically depend on absolute values of the model parameters. Rather, the coding properties of the network are mainly determined by the network structure and the relative weights and delays between different inputs.

Receptors

The population responses of low-frequency and high-frequency receptors are approximately linear within the dynamic range considered here (Imaizumi & Pollack, 2001; Ziehm, 2014). Consistent with a subtractive effect of the carrier frequency tuning on their intensity tuning, the tuning curves of individual receptors shift with carrier frequency, whereas the slope changes relatively little (Imaizumi & Pollack, 2001; Gollisch *et al.*, 2002). Intensity tuning broadens at 80 dB (Imaizumi & Pollack, 1999), justifying the choice of a relatively weak tuning of the receptor population.

Omega neuron 1

The ON1 receives input from low-frequency and high-frequency receptors (Hirtz & Wiese, 1997). Inputs from low-frequency receptors are slower than those from high-frequency receptors (Pollack, 1994; Faulkes & Pollack, 2000; Marsat & Pollack, 2004). This is consistent with the filters for 25 kHz peaking at approximately 4 ms earlier than those for 4.5 kHz (Fig. 4c). We made two simplifications regarding the action of ON1 in the network, neither of which affects our main conclusions. First, ON1 provides contralateral inhibition. For our monaural stimulation model, this would simply result in an attenuation of the inputs to ON1, which can easily be compensated for by increasing the synaptic weight of the inputs. Second, ON1 is inhibited by its contralateral mirror neuron. This inhibition appears to have little effect on the temporal pattern of ON1 responses and hence on its action on the two ANs (Marsat & Pollack, 2005). Data on ON1's timing of inhibition onto both ANs do not exist and to some extent depend on the intensity and location of sounds (Marsat & Pollack, 2005). However, for the stimulus conditions used in our experiments, it is reasonable to assume static synaptic delays.

Ascending neuron 1

The AN1 receives excitatory input from low-frequency receptors only (Hennig, 1988; Hirtz & Wiese, 1997) and inhibitory input from ON1 (Horseman & Huber, 1994; Faulkes & Pollack, 2001).

Ascending neuron 2

The AN2 receives inhibitory inputs from ON1 (Selverston *et al.*, 1985) and excitatory input from low-frequency and high-frequency receptors (Hennig, 1988; Hirtz & Wiese, 1997). Low-frequency inputs are much weaker than high-frequency inputs in driving AN2 (Hennig, 1988). Input from low-frequency receptors is slower than that from high-frequency receptors (Nolen & Hoy, 1987).

Cochlear model

We used a cochlear filter bank model from Zilany *et al.* (2009) to simulate a single fiber in the auditory nerve of the cat with a characteristic frequency of 2 kHz. In order to compare tuning at different SPLs with isolated tones, the model was probed with tones at different SPLs and the responses were normalised to the maximal response at each level. To estimate tuning from spectrotemporal receptive fields (Aertsen & Johannesma, 1981), the same model was stimulated with sparse dynamic random chords, played back at the same levels as the pure tones. For a detailed description of the stimuli and parameters see Linden *et al.* (2003). The density for all stimuli was 0.4 tones per octave. Tuning was extracted by fitting a spectrotemporal receptive field, collapsing it onto the frequency axis and normalising to maximal response.

Statistics

Data analysis and modeling were performed with custom-written routines in Matlab. Results are reported as mean ± SEM over specimens. We used a Kruskal–Wallis test with a Tukey–Kramer posthoc test (Matlab's multcompare) for multiple comparisons (across carrier frequencies), and we used a sign test for pair-wise comparisons (single-band vs. multi-band stimuli).

Results

Nonlinear summation of sound frequencies

To demonstrate the context-dependent integration of carrier-frequency channels in the cricket, we compared neuronal responses to stimuli with single and multiple carrier frequencies ('single-band' vs. 'multi-band' stimuli, Fig. 1a). We chose 4.5, 10, 15, and 25 kHz as carrier frequencies. This set of frequencies includes the whole range of ecologically relevant sounds: attractive, conspecific calling song (4.5 kHz) (Popov & Shuvalov, 1977), conspecific courtship song (10 and 15 kHz) (Libersat *et al.*, 1994), and aversive bat echolocation calls (25 kHz) (Marsat & Pollack, 2004). The AM of these single-band stimuli was random with a mean of 80 dB and a SD of 6 dB, resembling the stimulus statistics naturally encountered by crickets in the field (Marsat & Pollack, 2005). The two ANs were recorded using extracellular hook electrodes from the connective between the prothoracic and subesophageal ganglion (Fig. 1b) (Hennig, 1988). The local omega neuron ON1 was recorded using tungsten wire electrodes in the prothoracic ganglion (Marsat & Pollack, 2004) (Fig. 1b).

In a first step, we compared the mean firing rates in response to single-band stimuli with those measured when presenting the four carrier frequencies simultaneously (multi-band). If neurons summed the carrier frequencies linearly and did not perform context-dependent integration, the multi-band firing rates would equal the sum over frequencies of the single-band firing rates. All neurons responded consistently when stimulated with any of the four carrier frequencies at a mean intensity of 80 dB (Fig. 1c), indicating that all three neurons are sensitive to a broad frequency range at that intensity. Surprisingly, simultaneous presentation of all four carrier frequencies did not evoke higher firing rates than the presentation of the most effective carrier frequency alone, even though the multi-band stimulus exhibited much more stimulus energy. This observation indicates nonlinear integration across carrier frequencies in the cricket's auditory system.

Having examined the mean firing rates, we next looked at the temporal structure of spiking responses to the AM pattern in our stimuli. Responses of an AN2 to single-band and multi-band stimuli are shown in Fig. 1d. Although this cell type is mostly associated with high-frequency sound, the response of the cell is strongly modulated by the AM at all tested carrier frequencies (Fig. 1d). This is consistent with the mean firing rates exhibiting broad spectral tuning (Fig. 1c). Interestingly, when we stimulated AN2 with the multi-band stimulus, the response pattern often resembled the response to 15 and 25 kHz single-band stimuli, but rarely the response to low-frequency stimuli (Fig. 1d, green circles). In addition, some firing events that occurred upon stimulation with multi-band stimuli could not be correlated with any firing events found in the single-band responses, whereas some response peaks found in single-band responses did not appear in the multi-band response (Fig. 1d, purple bars). The latter occurred for almost all response peaks to single-band stimuli at 4.5 and 10 kHz, and less so at 15 and 25 kHz.

This further demonstrates the nonlinear integration of stimulus pattern across carrier frequencies and suggests that responses of AN2 to multi-band stimuli were mainly restricted to high carrier frequencies. Similar nonlinear integration across frequencies can be observed for the other two cell types in the network (AN1 and ON1; see Fig. 1c). However, as they exhibit less sparse responses (less clearly isolated firing events), these effects are less evident in the response pattern of these cells.

Having demonstrated the nonlinear and context-dependent integration of carrier frequencies in the cricket auditory system, we sought to (i) characterise spectrotemporal tuning in the cricket quantitatively, (ii) provide evidence for a role of context-dependent tuning in information transmission and (iii) propose putative mechanisms that may underlie this code.

Using spectrotemporal receptive fields to quantify spectrotemporal response properties

To thoroughly quantify the changes in spectrotemporal tuning with stimulus bandwidth suggested by firing rate tuning and firing patterns (Fig. 1c and d), we estimated from the responses a form of LN model known as spectrotemporal receptive fields (Fig. 2) (Aertsen & Johannesma, 1981).

Generally, LN models consist of a linear filter (Fig. 2b) and a static input–output function (nonlinearity, Fig. 2c) (Schwartz *et al.*, 2006). The filter describes neuronal selectivity for temporal stimulus features, whereas the nonlinearity converts the filtered stimulus to the neuronal firing rate. Spectrotemporal receptive fields are an extension of the standard LN model, in which each stimulus frequency band is allowed to have its own filter, i.e. the AM pattern (envelope) at each carrier frequency is filtered by an independent filter (Fig. 2a and b). The filtered envelopes are pooled and transformed by the nonlinearity to the cell's firing rate (Fig. 2d). The filter shape for each carrier frequency describes the carrier-frequency-specific selectivity for temporal envelope features, i.e. the temporal tuning. The filter magnitude or gain corresponds to the contribution of each carrier frequency to the firing rate and thus describes the spectral tuning.

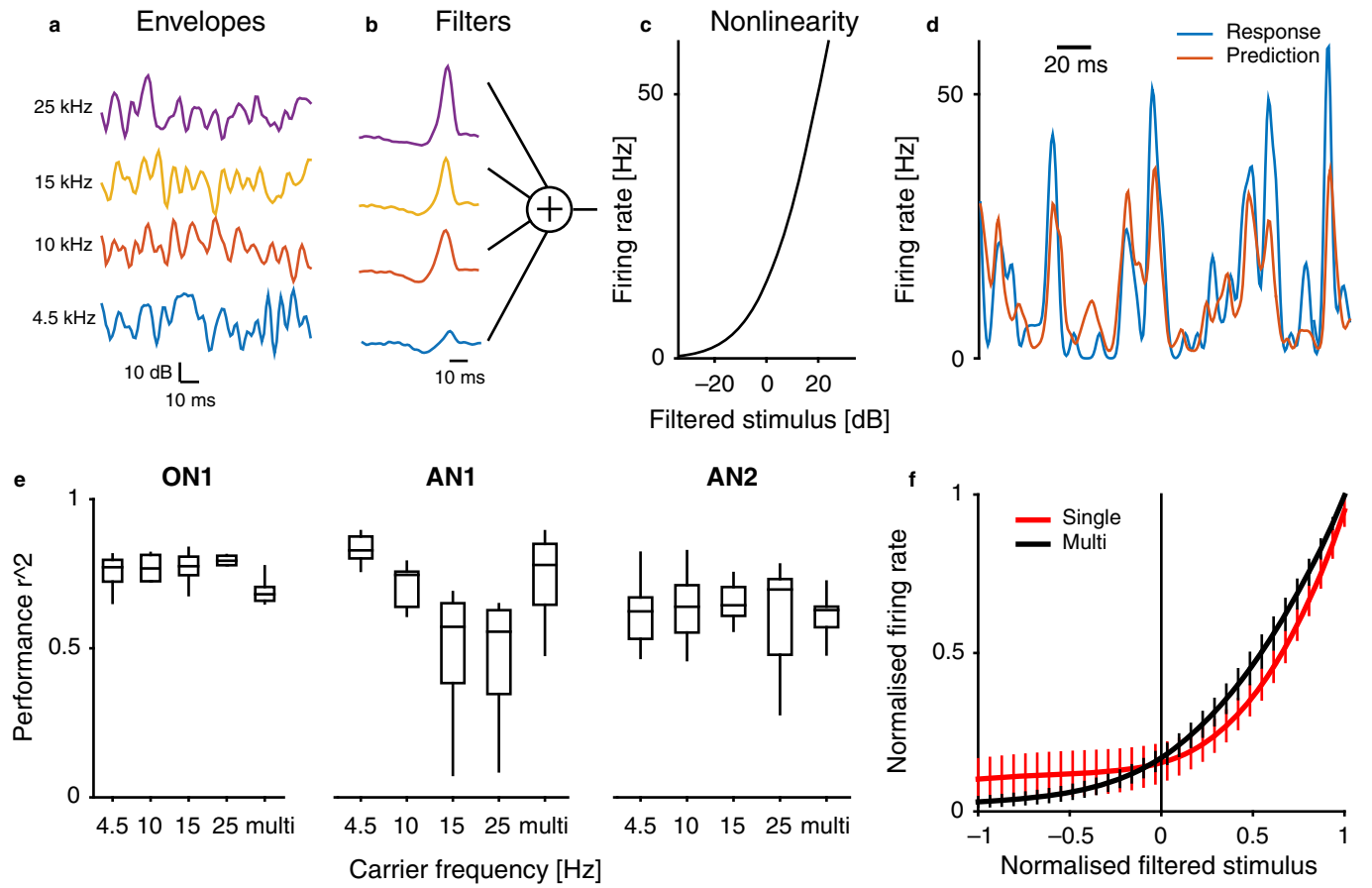

FIG. 2. Spectrotemporal receptive fields (STRFs) for cricket auditory neurons. (a–d) STRFs were fitted to neuronal responses to describe spectral and temporal tuning. The envelope of each carrier frequency (a) is filtered by a filter (b). Note that filters are read from right to left, e.g. the timing of the elicited spike is at the right. The filtered envelopes were then pooled and transformed by a nonlinearity (c) to the cell's firing rate (d). The filter shape for each carrier characterises the temporal tuning for that carrier, whereas the filter magnitude or gain corresponds to the spectral tuning (a carrier's contribution to the overall firing rate output). Shown are filters and predictions of AN2 for a multi-band stimulus. Match between response (blue) and prediction (red) in (d): r^2=0.75. (e) STRFs well describe neuronal responses in all three cell types and for all stimulus conditions. Box plots show r^2 between the experimental firing rate function and that predicted by the LN model for all recordings of each cell type. Performance is poorer for AN1 at 15 and 25 kHz because responses were relatively weak. (f) The STRF's nonlinearity (Fig. 1c) changes only little with stimulus condition. Shown is the nonlinearity averaged over all cells for the single-band stimuli (red) and the multi-band (black) stimuli (mean ± SEM). As different cells exhibited different firing rate levels and different filter scales, both values were normalised to their maxima before averaging cells.

We fitted LN models for single-band and multi-band stimuli and found that the models reproduced the response of all three cell types well (Fig. 2e). As the nonlinearity changed little across stimulus types in our data set, we restricted our analysis to the stimulus-dependence of the filters (Fig. 2f).

Adaptive changes of spectral tuning in the cricket

We first quantified stimulus-dependent spectral tuning by examining the filter gains. When probed with single-band stimuli, the filters of all three neurons in the network exhibit high gain at all carrier frequencies (Fig. 3a and b, red). This broad spectral tuning for single-band stimuli is consistent with the broad firing rate tuning (Fig. 1c).

For multi-band stimuli, the filter gain at each carrier frequency was reduced in all cells (Fig. 3b, black). This overall gain suppression reflects nonlinear integration across carrier frequencies as indicated by the firing rate tuning (Fig. 1c), as multi-band stimuli elicit a much smaller increase than expected from linear combination of the responses to single-band stimuli. Instead of explaining the firing rate tuning to multi-band stimuli by an overall reduction of a common gain, the LN models allowed us to quantify gain in a spectrally-resolved manner (Fig. 3b). For ON1, the reduction in gain was relatively uniform but strongest at 25 kHz; the spectral tuning of ON1 thus changed only little with stimulus bandwidth.

By contrast, spectral tuning drastically changed with stimulus bandwidth for both ANs, leading to a sharpening of tuning for multi-band stimuli in these cells (Fig. 3a, middle and right columns).

In AN1, the gain for 4.5 kHz did not change and the gain for 10, 15 and 25 kHz was strongly reduced (Fig. 3b, middle column). Spectral selectivity thus strongly increased for multi-band stimuli; AN1 became highly selective for calling song signals and disregarded temporal features at higher carrier frequencies.

The changes in spectral tuning of AN1 were complementary in AN2; a strong reduction of gain at 4.5 kHz and relatively small changes at the higher carrier frequencies led to this cell becoming tuned to high frequencies for multi-band stimuli (Fig. 3b, right column).

Thus, spectral tuning of all cells in the network was broad for single-band stimuli; selective gain reduction at complementary carrier frequencies sharpened tuning for multi-band stimuli in AN1 and AN2.

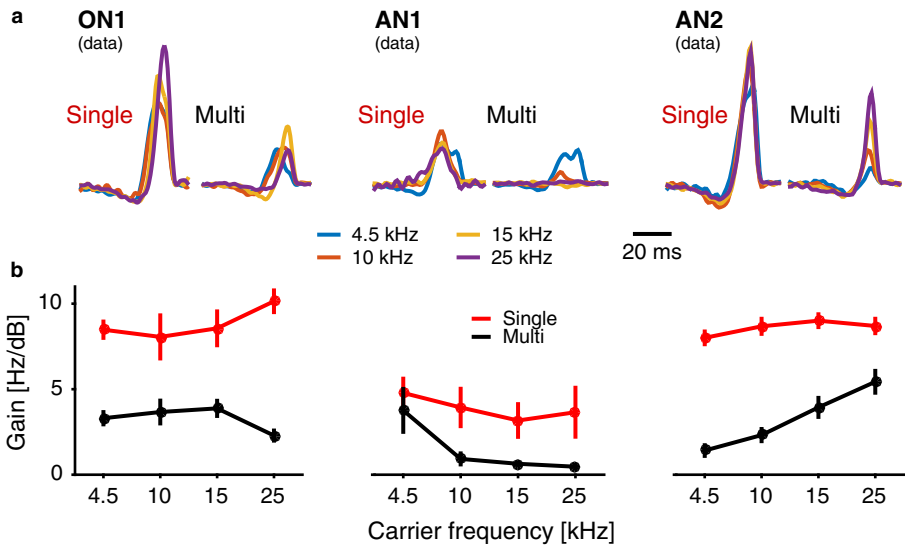

FIG. 3. Data. Adaptive changes of gain. (a) Filters for ON1 (left), AN1 (middle) and AN2 (right) for single-band and multi-band stimuli. Shown is the average over recordings. For error bars see Fig. 4, they are omitted here for clarity. Carrier frequency is color-coded as indicated in the legend. (b) Carrier-specific gain for ON1, AN1 and AN2 in the model for single-band (red) and multi-band (black) stimuli. All cells exhibited an overall reduction of gain for multi-band stimuli, except AN1 at 4.5 kHz. Shown is the mean ± SEM over all recordings for each cell.

Temporal tuning is decorrelated adaptively

After comparing the spectral tuning by means of the filter gain at different carrier frequencies, we next investigated the role of temporal tuning in mediating adaptive coding. To this end, we compared the filter shapes of auditory neurons in response to single-band or multi-band stimuli (Fig. 4).

For single-band stimuli, filters for all cell types exhibited a dominant positive peak and only a weak negative lobe (Fig. 4a, red). Thus, all cells were mainly low-pass filters of the envelope at each carrier frequency (spectral transfer function exemplified for AN2 in Fig. 4d, red trace).

The temporal selectivity of ON1 changed only little for multi-band stimuli (Fig. 4a, top row; Fig. 4b, left). The greatest difference was in the timing of the filter peak for 4.5 kHz, which was further delayed relative to 25 kHz (Fig. 4c) (cf. Marsat & Pollack, 2004).

In contrast to ON1, the filter shape for the two ANs changed drastically. As in our observation for the spectral tuning, these changes affected the low-frequency and high-frequency bands in AN1 and AN2 in a complementary manner (Fig. 4a, middle and bottom rows, compare Fig. 3b).

For AN1, the filter for 4.5 kHz was unaltered. However, the filter for 10 kHz revealed a weak reduction in amplitude and the filters at 15 and 25 kHz lacked any clear structure (Fig. 4a, middle row; Fig. 4b, middle). Some specimens of AN1 (2/6) even lacked a well-structured filter for single-band stimuli at 15 and 25 kHz, probably because of a sharper tuning or less sensitive low-frequency receptors (not shown).

For AN2 and multi-band stimuli, the filters at high carrier frequencies remained largely unimodal, whereas the filter for 4.5 kHz acquired a bimodal shape (Fig. 4a, bottom row; Fig. 4b, right). This entailed a striking transformation of the coding properties from a low-pass to a band-pass filter (Fig. 4d). The non-normalised filter suggested that this transformation was mainly through a reduction of the positive lobe ('excitation'), not an increase in the magnitude of the negative lobe ('inhibition') (Fig. 3a, right). In some recordings of AN2 (4/12), the filter at 4.5 kHz became strictly negatively lobed.

Thus, our experiments demonstrate adaptive and complementary sharpening of tuning in the output neurons of the cricket's peripheral auditory system (Figs 3 and 4): spectral tuning of AN1 became more selective for 4.5 kHz, whereas the temporal tuning changed only little with stimulus condition. In AN2, the tuning for carrier frequency became more high-pass; the temporal filter for the envelope at 4.5 kHz changed from a unimodal to a bimodal shape, whereas those for high carrier frequencies did not change.

Given the small numerical size of the cricket auditory system, we were surprised by such profound changes in coding properties. Having thoroughly quantified context-dependent spectrotemporal tuning using spectrotemporal receptive fields, we aimed to (i) provide evidence that context-dependent coding improves information transmission and (ii) propose putative mechanisms that could underlie nonlinear coding in neural networks.

Adaptive spectrotemporal tuning preserves information

The changes in spectrotemporal tuning with stimulus condition mainly involved a gain reduction for some input frequencies (AN1 and AN2; Fig. 3) or a reduction in the bandwidth of the filter from low-pass to band-pass (AN2; Fig. 4). Although this sharpening of tuning increases specificity, it also entails a loss of information; broad tuning has the potential to encode all inputs, whereas a carrier frequency subject to gain reduction will not be encoded anymore. To explore whether sharpening of tuning is detrimental to information transmission or whether it has a beneficial role, we used an optimal linear decoder and investigated how much information about each carrier frequency can be recovered from the neuronal response. We started by exploring the problem of coding multiple inputs in a setting where we have perfect control over the changes in coding properties; using a simple, normative model we demonstrate how a neuronal system should change its coding properties to optimise information transmission (Massot *et al.*, 2012; Middleton *et al.*, 2012). We then used our experimental data to test the predicted effects in information transmission.

The normative model investigates the trade-off that the cricket auditory network faces in a generalised framework; like AN2, the model receives input on two carrier-frequency channels and encodes

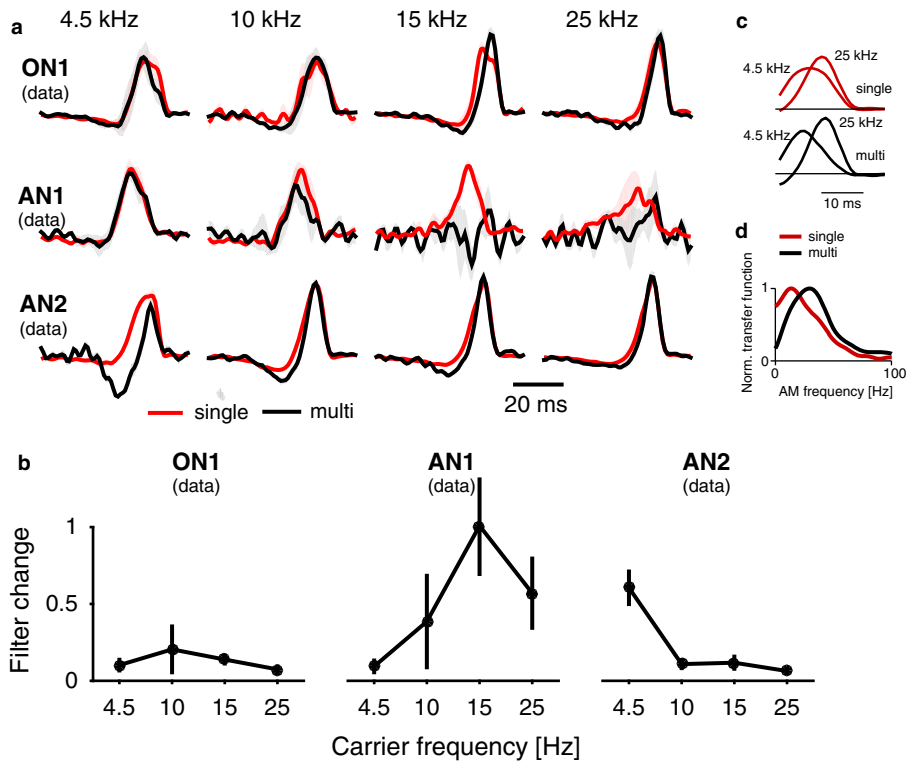

FIG. 4. Data. Adaptive changes in filter shape. (a) Filters for ON1, AN1 and AN2 (rows) for different carrier frequencies (columns) when presented alone (single band, red) or as a sum (multi-band, black). Lines correspond to mean and shaded areas depict SEM over specimens for each cell type. For the plots, experimental filters were normalised to unit norm for better visibility. Original filters are shown in Fig. 3a. Variability of filter shape for AN1 at 10, 15 and 25 kHz was relatively large as the individual filters lacked reproducible structure. Otherwise, variability is small due to high response stereotypy across specimen. (b) Changes in filter shape when comparing filters estimated from single-band and multi-band stimuli for ON1, AN1 and AN2 (error bars indicate SEM over specimens). Change was calculated as 1 minus the dot product of the normalised individual filters for each condition and carrier frequency (see Materials and methods). (c) Time course of the filters for ON1 (average over all recordings) at 4.5 and 25 kHz for the single-band and multi-band condition. The filter for 4.5 kHz rises more slowly than that for 25 kHz; this delay is increased for multi-band stimuli. (d) Transfer function (AM frequencies) for AN2 at 4.5 kHz for the single (red) and multi-band (black) condition. Graphs were normalised to a maximum at 1.0 for better comparison of the overall shape. For the multi-band conditions, the filter becomes more band-pass as responses to low frequencies are reduced.

information about the AM pattern of the individual inputs. Each input is filtered and thresholded. The model output is obtained by pooling the response to each input channel (Fig. 5a). We then searched for filter shapes and gains that maximise information transmission.

For a single-band input, the model transmits 110 bits/s of information (Fig. 5b). Interestingly, this baseline value is reduced to 80 bits/s when the model encodes two inputs simultaneously (Fig. 5c), i.e. not only is the information about each individual input reduced but also total information is lost. This is caused by ambiguity; given only the pooled response, it is not clear which part of the response corresponds to which of the two inputs, as the response components lack a label marking them as coming from either input (Clemens *et al.*, 2011). Even worse, for reconstructing one of the two inputs, the response elicited by the other input constitutes noise, leading to a further loss of total information.

If we reduce the gain of one of the inputs as seen in AN1 and AN2 (Fig. 3b), information about the suppressed input is nearly lost (3 vs. 40 bits/s, Fig. 5d). However, this loss of information about one of the inputs leads to an increase of information about the other input (40 vs. 101 bits/s) and also in terms of total information (104 vs. 110 bits/s). Thus, the gain reduction in AN1 and AN2 focuses coding to specific inputs and improves overall information transmission.

Changing the bandwidth of the filters for one of the inputs is a second way to implement contextual coding (Fig. 5e). Here, the transformation of the filter transfer function (low-pass to band-pass as in AN2; Fig. 4a, lower left) entails a reduction of information about low AM frequencies. Now only the low AM frequencies of input 1 and the high AM frequencies of input 2 are encoded (Fig. 5e, middle row). Thus, reducing the similarity of both filters as in AN2 leads to a preservation of total information.

The normative model illustrates that, instead of leading to an overall information loss, the sharpening of tuning in AN1 and AN2 can preserve information by reducing the overlap between the representations of concurrent inputs. In the case of gain suppression, this is accomplished by tuning out one of the inputs. In the case of the filter shapes, it is achieved by encoding complementary aspects of the inputs. Hence, the changes in filter shapes (Fig. 4) and gain (Fig. 3) observed in the cricket auditory system could help to preserve information when multiple inputs are present.

To directly demonstrate that the adaptive changes in coding improve information transmission, we estimated information from our experimental data. Using an optimal linear decoder (see Materials and methods) we compared the information about the AM pattern at each carrier frequency for single-band and multi-band stimuli.

In ON1, we observed a loss of information in the multi-band condition across all frequencies (Fig. 5f and g). This is consistent with the predictions of the normative model (Fig. 5c), as ON1's spectrotemporal tuning did not adapt, i.e. it was broad for single-band and multi-band stimuli (Fig. 3c). Hence interference and

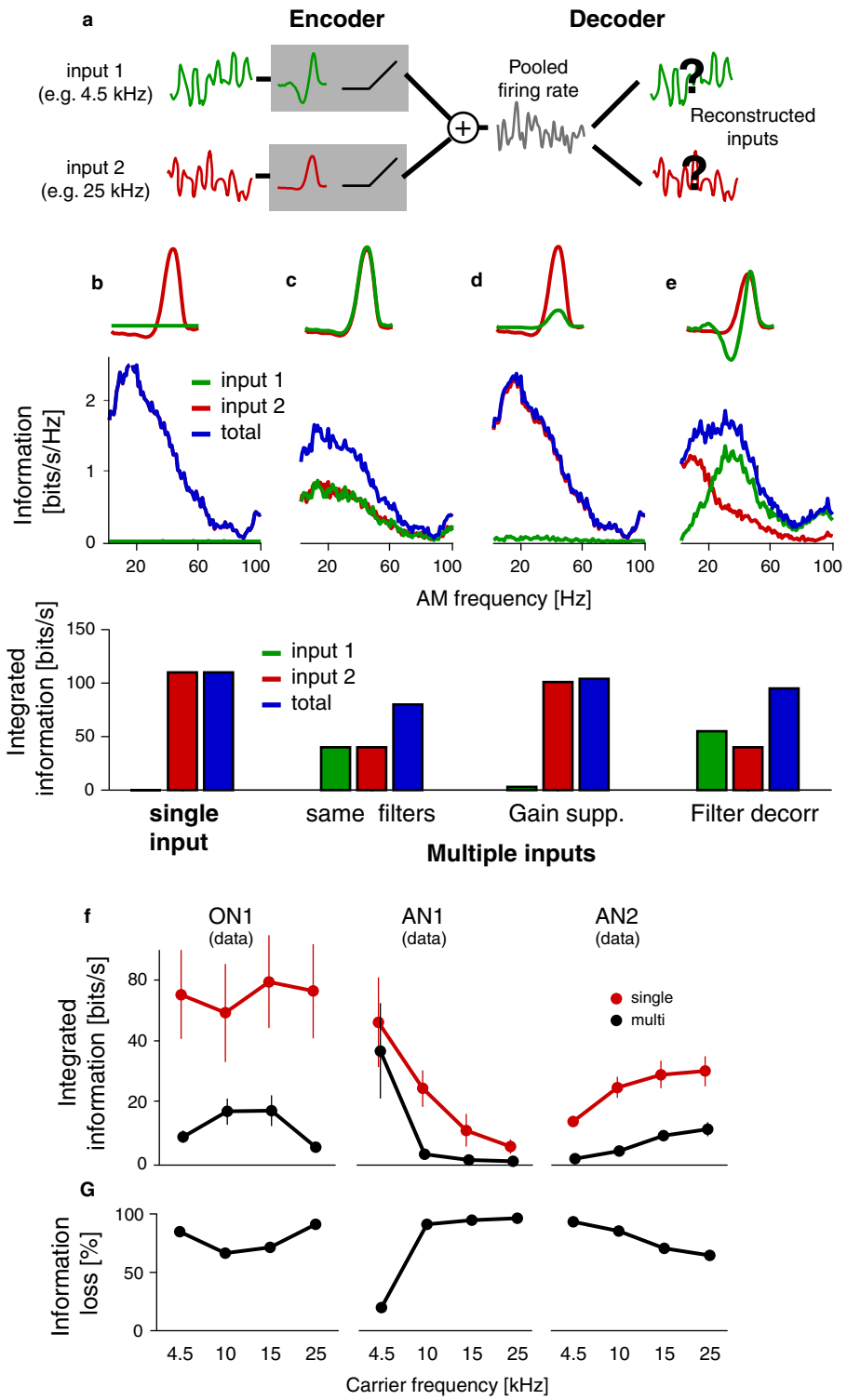

FIG. 5. Model. Encoder–decoder model and the effect of suppression and decorrelation of filters on information tuning. (a) We modeled information transmission in a single neuron receiving two time-varying inputs (green and red lines, respectively). Each input trace was filtered and thresholded independently (gray boxes) before being pooled (gray trace). We then investigated how much information an optimal linear decoder can extract from the pooled response about the individual input patterns. (b–e) The top row of each panel shows the filters for each of the two input channels. The middle row depicts the information of the decoder as a function of AM frequency for each input channel (green and red lines) and the total information of the decoder (blue lines, sum of green and red lines). Bars plots in the bottom row show the overall information integrated between AM frequencies 1 and 100 Hz. Four different cases were modeled: (b) the decoder received one input only; (c) the decoder received two inputs with identical filters for both inputs; (d) one filter was suppressed; and (e) one filter was changed to a band-pass. (f) Coherence information in the recorded responses for ON1, AN1 and AN2 about the envelope of different carrier frequencies when presented in isolation (single, red) and as a mixture (multi, black). All plots show mean ± SEM. (g) Loss of information. Shown is the difference of the information values plotted in (f).

ambiguity between all carrier frequencies was strong and information was lost.

By contrast, information was preserved in AN1 for 4.5 kHz and information was lost only at higher carrier frequencies (Fig. 5f and g). This is consistent with the effect of strong gain suppression for higher frequencies (Fig. 3b) predicted by the normative model (Fig. 5d). Thus, nonlinear integration of inputs in AN1 selectively preserved information about conspecific communication signals.

In AN2, information about AM was partly lost for all carrier frequencies when presented simultaneously (Fig. 5f and g, right). However, when we compared how much information was degraded by the presence of other frequency bands, we found differences between low and high frequencies. In AN2, 93% of the information about 4.5 kHz was lost during multi-band stimulation, whereas for 25 kHz, information was reduced by only 64% (Fig. 5f and g, right). Thus, nonlinear coding in AN2 [gain suppression and changes in filter shape (Figs 3b and 4b)] reduced information loss about the AM pattern of high frequencies in a multi-band stimulus, in agreement with its role for high-frequency predator signal coding.

Information theory thus provided a functional explanation for the changes in spectrotemporal coding. The interference among carrier frequencies due to the broad tuning of single neurons in the single-band condition was avoided by the selective preservation of information about either conspecific (AN1) or predator (AN2) signals in the multi-band condition.

A network model suggests mechanisms underlying adaptive spectrotemporal coding

Our analysis revealed two types of adaptation that both preserve information transmission for multi-band stimuli (Fig. 5): selective reduction of gain and changes in filter shape (Figs 3 and 4). Similar context-dependent codes have been described in much more complex sensory systems (e.g. Gourévitch *et al.*, 2009). Interestingly, the well-characterised cricket auditory pathway constitutes a minimal instantiation of a common network motif (broadly-tuned feed-forward inhibition) as ON1 pools information from both receptor populations and inhibits both ANs (Wohlers & Huber, 1982; Selverston *et al.*, 1985; Horseman & Huber, 1994).

To formulate testable hypotheses about the mechanisms underlying adaptive spectrotemporal coding, we built a network model inspired by the structure of the cricket auditory system. Our minimal circuit model of the auditory system of crickets included two receptor populations (low-frequency and high-frequency), the inhibitory local neuron ON1, and AN1 and AN2 (Fig. 6). The neurons were linear rate units and the synapses were linear with a weight and a delay. Model parameters were taken from the literature if available (see Materials and methods for details). For some of the parameters, we made biophysically reasonable assumptions to ensure that the model reproduced the data (Table 1). Our data set describing the spectral and temporal tuning of the three major neurons in the network for different stimulus conditions constituted a powerful constraint for model parameters. Moreover, we ensured that the results did not depend on the specific parameter values.

The source of the adaptive spectral tuning in the model is a logarithmic input nonlinearity

In our experimental data, we observed stimulus-dependent spectral tuning, mediated by a suppression of gain for nonpreferred frequencies (Fig. 4). We tested our network model with the same single-band and multi-band stimuli and repeated the LN model analysis with the result of the model simulation by looking at changes in filter shape and gain with stimulus bandwidth. Even though the network model explicitly excluded adaptive mechanisms or dynamic changes in its parameters, it achieved the adaptive firing-rate tuning

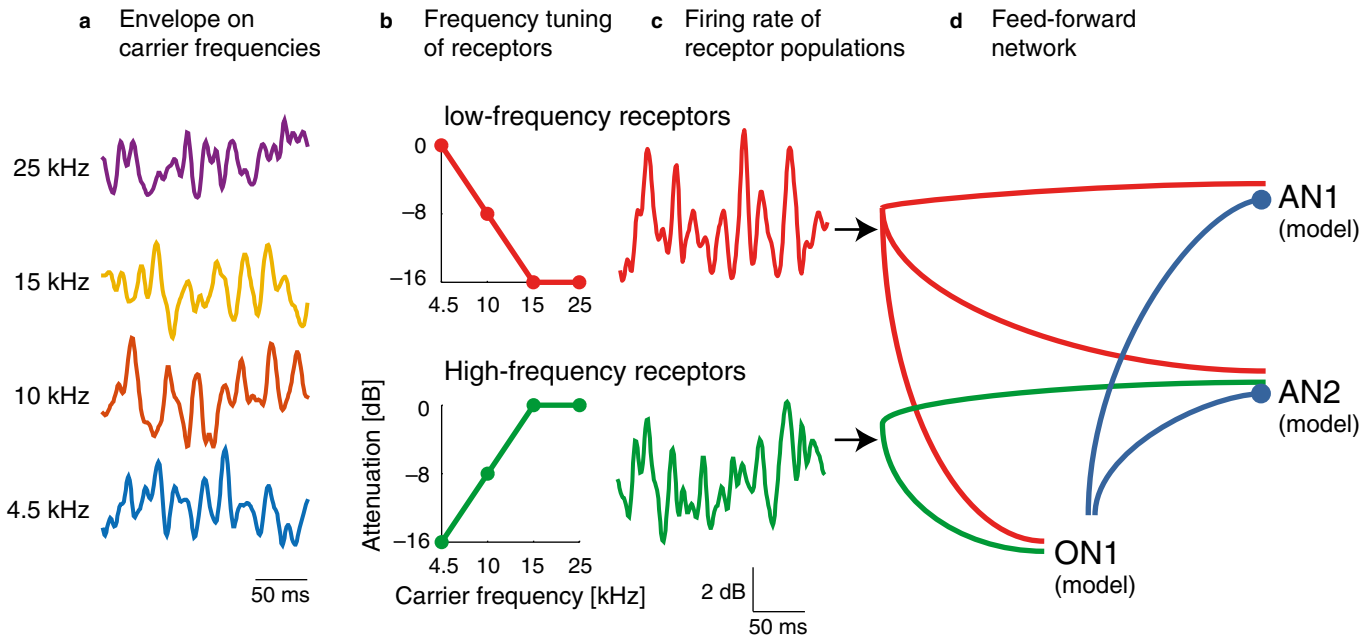

FIG. 6. Network model inspired by the early auditory system of the cricket. (a) Random envelope of the four carrier frequencies provides input to the network. (b) Two populations of receptors are relatively broadly tuned, most sensitive to either low or high carrier frequencies. (c) The receptor populations transform the envelope to a firing rate. Traces show the firing rate resulting from integrating the inputs across carriers shown in (a). (d) The network integrates inputs from low-frequency and high-frequency receptors (red and green lines, respectively). AN1 receives excitatory input only from low-frequency receptors. AN2 is excited by both receptor populations. ON1 pools input from both receptor populations and inhibits AN1 and AN2 (blue lines). See Materials and methods for details.

(Fig. 7c, compare Fig. 1c) and the adaptive spectrotemporal tuning qualitatively similar to the experimental observations (Fig. 7a and b, compare Fig. 3a and b). As the model reproduced our experimental data, we were able to explore the mechanisms behind context-dependent adaptation in the network model by selectively changing individual components.

The most obvious candidate mechanism for adaptive coding is the inhibition mediated by ON1, as this neuron receives input from both receptor populations and thereby constitutes a global gain-control pool (Wohlers & Huber, 1982; Pollack, 1994). Surprisingly, removing the inhibitory inputs from ON1 to both AN1 and AN2 had little effect on the shape of the spectral or firing rate tuning (Fig. 7b and c, compare black and green lines).

Having ruled out ON1 as the primary origin of context-dependent spectral tuning in the model, we concluded that the effect must arise earlier, i.e. in the auditory receptors. Indeed, the receptors in the network model already displayed the adaptive spectral tuning in AN1 and AN2; it was broad for single-band stimuli and followed their input frequency tuning only for multi-band stimuli [shown here for low-frequency receptors (Fig. 7d), high-frequency receptors exhibit similar behavior].

These changes in tuning did not result from changes in network model parameters; the parameters determining receptor tuning were the same across stimulus conditions (Fig. 6b). Stimulus-dependent tuning was thus an emergent property created by static nonlinearities in the network. The main nonlinearity in the model was the transformation from the pressure to the decibel scale and replacing this logarithmic nonlinearity with a linear transformation did abolish adaptive tuning; now, all carrier frequencies exhibited differential gain according to the frequency tuning of the receptors in all stimulus conditions (Fig. 7d). This adaptive effect of the pressure-to-decibel transformation did not rely on a specific functional form provided it was saturating. We observed a similar effect with power law or exponential-like nonlinearities commonly used to fit the input–output functions of sensory receptors in other modalities (Fig. 7f–g). Given that saturating nonlinearities are relatively common, they could support adaptive codes in many neural systems.

To further validate the generality of the finding that a saturating input nonlinearity enables adaptive tuning, we tested the spectral tuning of a standard model of the mammalian cochlear filter bank (Zilany *et al.*, 2009) using single-band or multi-band stimuli. This model is equipped with a logarithmic input nonlinearity and accordingly exhibits a sharpening of tuning for multi-band stimuli (Fig. 7h, compare red and black tuning curves). To our knowledge, such adaptive spectral tuning in the cochlea has not been noted before. This suggests that the sharpening of tuning observed in more central auditory areas in the mammalian brain (Gourévitch *et al.*, 2009) could be a consequence of static nonlinearities already within the cochlea.

Decorrelation of temporal tuning in the model is governed by the strength and timing of inhibition

We next used the network model to investigate the context-dependent temporal tuning AN1 and AN2 (Fig. 4). The filter changes observed for single-band and multi-band stimuli in the neurons of the network model corresponded well with those seen in the data (compare Figs 8a and 4a). As in the data, these changes were largely confined to the carrier frequency that underwent the strongest gain suppression (compare Figs 3 and 4).

Although the logarithmic nonlinearity of the receptor population provided a mechanism for changes in spectral tuning, it could not explain the observed filter changes. However, although inhibition did not contribute to spectral tuning (Fig. 7b), the interplay of excitation and inhibition could be the mechanism behind the adaptation of temporal coding. Indeed, removing inhibitory inputs from ON1 to both AN1 and AN2 abolished the observed changes in filter shape with stimulus condition (Fig. 8b, compare Fig. 4b).

The effect of inhibition on filter shape can be directly visualised as our network model is linear; the output filters of individual neurons thus arise from simple linear summation of their input filters. For example, the filter of AN1 is the combination of the filter of low-frequency receptors and of ON1, each weighted and delayed by the parameters of the associated synapse (Fig. 9b). We reasoned that the changes in filter shapes arise from an increase in inhibitory drive induced by multi-band stimuli. We thus quantified the excitatory or inhibitory drive by the integral of the weighted filters with positive and excitatory synaptic weights, respectively, and then calculated the ratio of total inhibitory and excitatory drive (I/E ratio). Small I/E ratios indicate weak inhibition, whereas ratios close to 1 indicate the even strength of excitatory and inhibitory inputs.

The I/E ratio is uniform across frequencies and small in AN1 and AN2 for single-band stimuli, indicating that excitation far outweighs inhibition for this stimulus condition (Fig. 9a, red). By contrast, the I/E ratio differs between carrier frequencies for the multi-band stimulus. Most notably, at carrier frequencies whose gain is strongly suppressed (Fig. 3b), the I/E ratio increases and approaches values of 1.0, indicating balanced excitatory and inhibitory inputs (AN1 at 15 and 25 kHz, AN2 at 4.5 kHz, Fig. 9a). These are the same carrier frequencies at which the filter shapes change the most; hence, the magnitude of the filter changes is largest at frequencies where the relative strength of inhibition increases most strongly (compare Fig. 8b). Note that we did not change any of the model parameters with stimulus condition. These changes in the effective inhibitory drive thus emerge from the network connectivity and the logarithmic input nonlinearity in receptors.

The I/E ratio thus explains the magnitude of filter shape changes at each carrier frequency with stimulus bandwidth. However, the nature of this change was different in each AN (Fig. 4a) despite the I/E ratio being similarly close to 1.0 in both cases (Fig. 9a). In AN1 at 15 and 25 kHz, we observed a loss of any filter structure, whereas in AN2 at 4.5 kHz, the filter changed from unimodal to bimodal (Fig. 4a). The timing of excitation and inhibition can explain these effects. In AN1 at 15 and 25 kHz, excitation and inhibition are coincident (Fig. 9b, left, red and blue, respectively). As they are both approximately balanced for multi-band stimuli (Fig. 9a), they cancel each other, leading to an almost flat filter (Fig. 9b, right, black). By contrast, in AN2 at 4.5 kHz, excitation slightly led inhibition (Fig. 9b, red and blue). For single-band stimuli, the inhibitory drive was too weak to strongly affect filter shape in AN2 and hence the filter was shaped primarily by the unimodal filters of excitatory inputs (Fig. 9c, left). However, with inhibition being much stronger for multi-band stimuli (Fig. 9a, right), a negative lobe emanates due to inhibition initially outweighing excitation (Fig. 9c, right).

In summary, our network model suggests two putative mechanisms enabling adaptive spectrotemporal tuning, i.e. a saturating input nonlinearity can produce adaptive spectral tuning and alters the relative strength of inhibition. This change in I/E balance then leads to changes in temporal tuning whose specific nature depends on the timing of inputs.

Discussion

We proposed that sensory coding should change adaptively, depending on whether a stimulus is presented alone or together with other stimuli. For the cricket auditory system studied here, tuning should

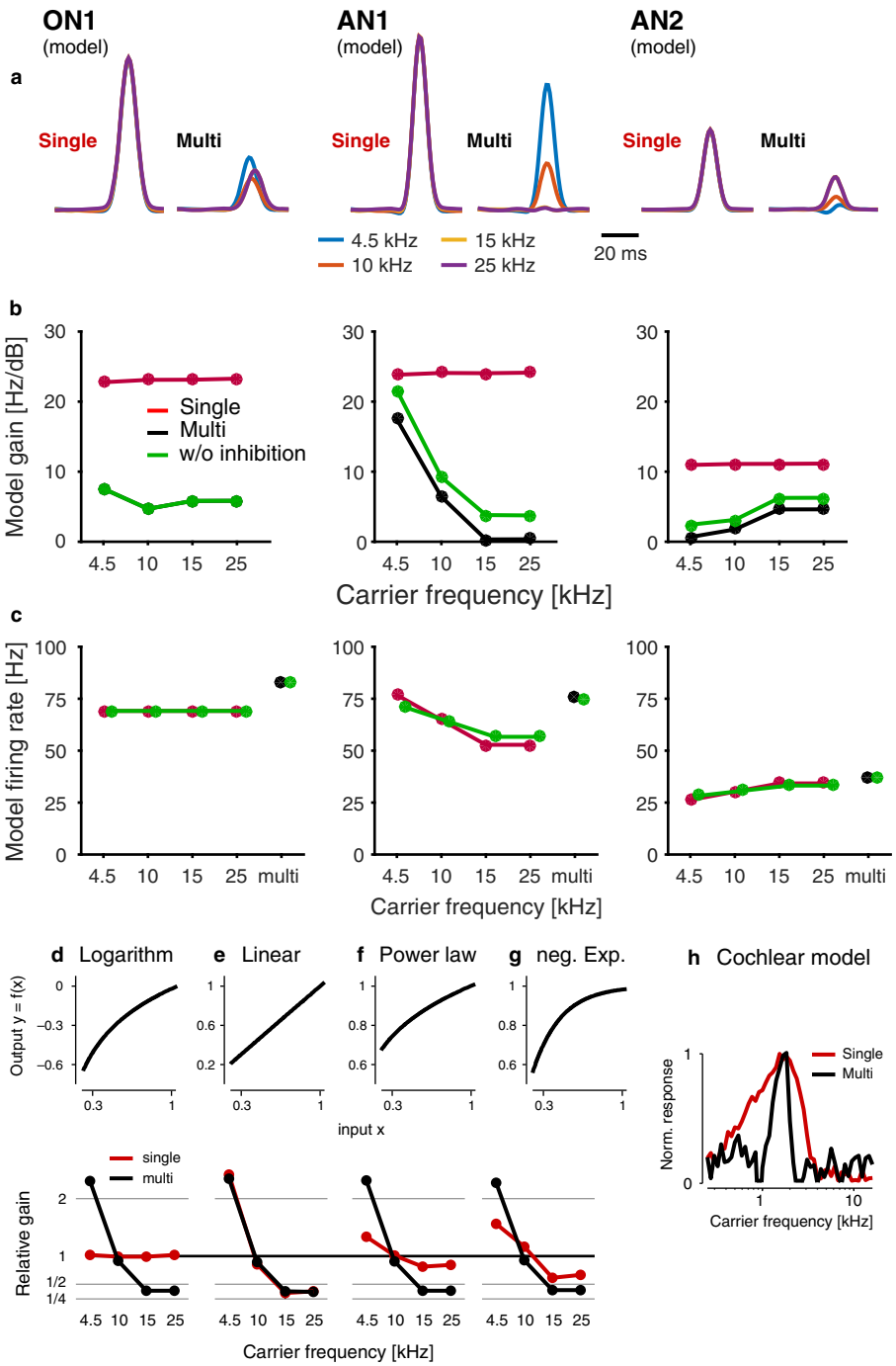

FIG. 7. Model. Adaptive gain: the impact of inhibition and of input nonlinearities. (a) Filter (nonscaled) for ON1, AN1 and AN2 in the network model for single-band and multi-band stimuli (compare with data in Fig. 3a). (b) Gain of the filters in (a) for single-band (red) and multi-band (black) stimuli (compare with Fig. 3b). Green curves show gain of a model without (w/o) inhibition from ON1 to AN1 and to AN2. (c) Mean firing rates in the network model for the different stimulus conditions (single, red; multi, black; without inhibition from ON1, green) (compare with Fig. 1c). (d–g) Different types of nonlinearities (top) and the resulting relative gain (bottom) of low-frequency receptors for single-band (red) and multi-band (black) stimuli: (d) logarithmic nonlinearity as in the network model $y = \log(x)$; (e) linear $y = x$ (f) power law $y = x^{1/4}$; (g) negative exponential $y = 1-\exp(-4x)$. (h) Tuning of a standard filter bank model of the mammalian cochlear stimulated with single tones (red) or dynamic random chords (black) (see Materials and methods).

then change from integration across frequency channels to selective encoding of an individual channel. Consistent with this prediction, we found that the spectrotemporal tuning of cricket auditory neurons narrows when challenged with broadband stimuli (Figs 3 and 4). This adaptive tuning improves information transmission (Fig. 5) and may be implemented by a saturating input nonlinearity and feed-forward inhibition (Figs 7–9).

Decorrelated coding maximises information about individual stimulus components by reducing interference

Information theoretical studies show that, when encoding simple stimuli consisting only of a single component, neurons in a population should have broad, overlapping tuning curves to exploit all available coding capacity (Pouget *et al.*, 1999; Zhang & Sejnowski,

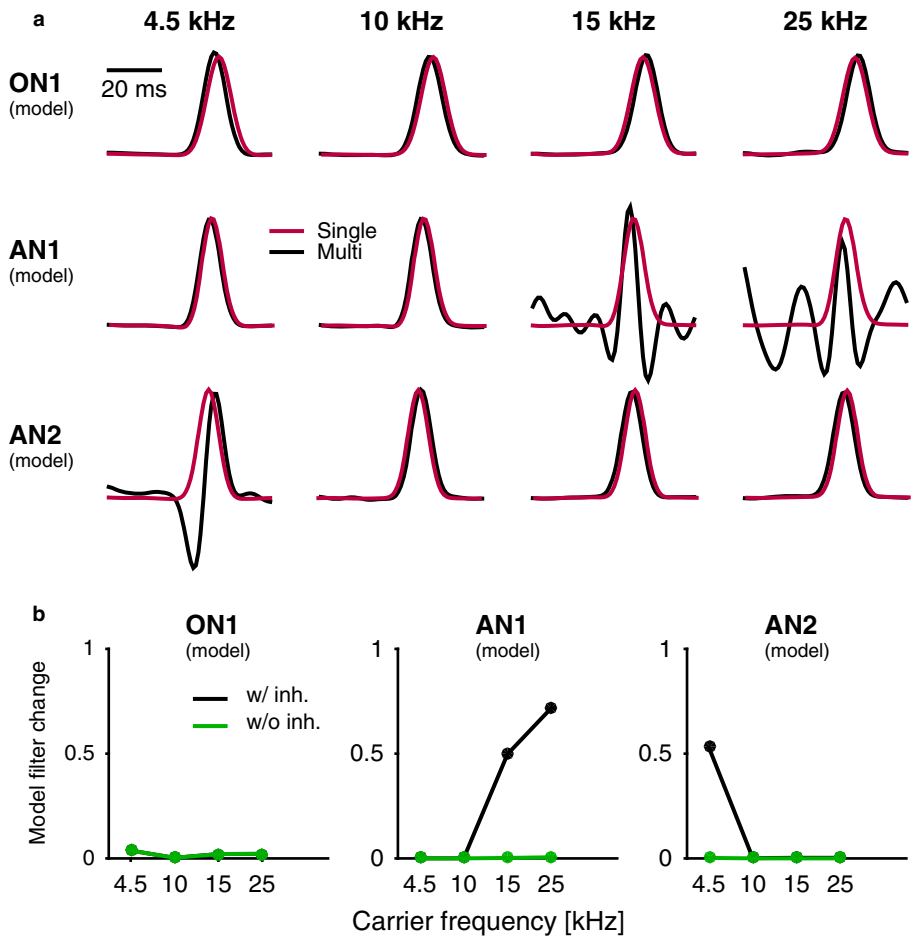

FIG. 8. Model. Adaptive temporal selectivity and the role of inhibition. (a) Filters in the network model for single-band (red) and multi-band (black) stimuli. Filters change with stimulus condition as seen in the data (compare with Fig. 4a). (b) Changes in filter shape for ON1, AN1 and AN2 in the network model for multi-band stimuli (compare black lines with Fig. 4b; see Materials and methods for details on the quantification of filter changes). Green curves show the changes in filter shape in a model without inhibition (w/o inh.) from ON1 to AN1 and AN2. w/ inh., with inhibition.

1999; Seriès *et al.*, 2004). By contrast, tuning should sharpen for encoding multiple, concurrent stimuli (Fig. 5) (see also Massot *et al.*, 2012; Middleton *et al.*, 2012). As stimulus conditions can vary between these two cases, a neural system needs to rapidly change its tuning from broad for single stimulus components to narrow for multi-component stimuli to maintain optimal coding. This leads to stimulus-dependent tuning, known from many systems [electric fish (Chacron *et al.*, 2003), rodent auditory cortex (Ahrens *et al.*, 2008), primate visual cortex (Vinje & Gallant, 2000) and primate vestibular system (Massot *et al.*, 2012)]. The adaptive spectral and temporal tuning observed in the cricket is consistent with this view (Figs 3 and 4). For single-band stimuli, AN1 and AN2 exhibited broad and similar spectral and temporal tuning. For multi-band stimuli, spectral sensitivity narrowed, thus restricting each AN to encode only a subset of carrier frequencies present in the multi-band stimulus (Fig. 3b). These subsets of carrier frequencies are defined in terms of the behavior elicited by them, i.e. either approach to low calling song frequencies (4.5 kHz in AN1) or avoidance of high-frequency predator signals (15 and 25 kHz, AN2).

The changes in spectrotemporal tuning affected complementary ranges of carrier frequencies in the two ANs. This decorrelated the spectrotemporal receptive fields across both ANs and potentially reduced stimulus-driven correlations in responses to broadband stimuli (Figs 3 and 4). Decorrelation of receptive fields has been discussed in the context of redundancy reducing codes (Vinje & Gallant, 2000; Barlow, 2001). In our case, decorrelation has a different role; it leads to different stimulus components being transmitted through separate channels (AN1 and AN2). This reduces interference between the representations of co-occurring signals (Fig. 5) and simplifies the neural code as it avoids having to decompose the multiplexed representation of different components upon readout. Moreover, this organisation of adaptive coding at the network level (with complementary ranges of carrier frequencies being suppressed) helps mitigate the information loss entailed by an increase of specificity, i.e. a narrowing of tuning (Fig. 5d and e). This suggests that information is not only maximised in single cells but also at the population level.

Stimulus-dependent coding and gain control

The adaptive coding in the cricket is reminiscent of 'max-like' as opposed to 'average-like' or 'summation-like' encoding of multiple stimulus components (Wimmer *et al.*, 2008). That is, both AN1 and AN2 preferentially responded to the strongest inputs in a mixture, rather than to the average or sum of all components (Fig. 3) [compare Gawne & Martin (2002) with Zoccolan *et al.* (2005) and Carandini & Heeger (2012)]. This seems efficient, as AN1 or AN2 should not encode the compound envelope across all carrier frequencies, as the temporal pattern at different carrier frequencies conveys different categorical meaning to the cricket (Wyttenbach *et al.*, 1996). Facing a similar problem, a motion-sensitive neuron in area middle temporal of

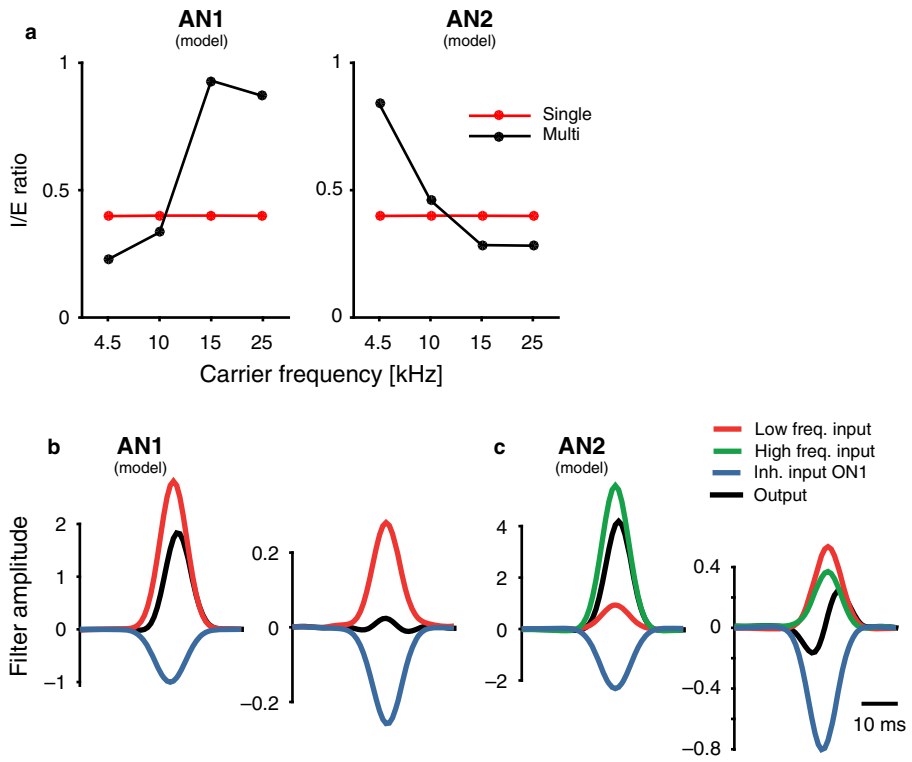

FIG. 9. Model. Adaptive temporal selectivity and the role of inhibition. (a) Ratio between inhibitory and excitatory drive (I/E ratio) to AN1 (left) and AN2 (right) in the model. Inhibitory/excitatory drive is given by the integral of the weighted filters of inputs with inhibitory/excitatory synaptic weights. While the I/E ratio is uniform for single-band stimuli (red), it becomes carrier-frequency dependent for multi-band stimuli (black). (b and c) Role of the strength and timing of inhibition in creating adaptive temporal selectivity in the network model. Generation of the filter shapes (black traces) in AN1 (b) and AN2 (c). Shown are the model filters for the inputs, multiplied by the synaptic weight and delayed by the synaptic delay (low-frequency receptors, red; high-frequency receptors, green; ON1, blue) and their changes with stimulus condition (left, single-band; right, multi-band). The resulting filters are the sum of the weighted and delayed input filters. Delays are relative to the spike, hence left-shifted filters indicate an increase in the delay. (b) The filter of AN1 at 15 kHz is generated by combining the filters of the excitatory (red, low-frequency receptors) and inhibitory (blue, ON1), each modified by the synaptic weight and delay. For single-band input (left), excitation (red) outweighs inhibition (blue), producing a positive output filter for AN1. For multi-band inputs (right), excitation (red) and inhibition (blue) are balanced and cancel each other to form the flat output filter of AN1 (black). (c) Same as in b but for AN2 at 4.5 kHz. Inputs to AN2 are low-frequency (red) and high-frequency (green) receptors and inhibition from ON1 (blue). Excitatory inputs outweigh inhibitory inputs for single-band inputs (left). For multi-band stimuli, excitation (red and green) and inhibition (blue) are balanced and, due to different delays, create a bimodel output filter (black).

the primate visual pathway should not respond to the average motion of two divergent objects in the visual field. Max-like or winner-take-all encoding is one outcome of the divisive normalisation observed in more complex sensory systems like the primary visual cortex. The fact that we find a similar computation in a much simpler system suggests that gain control is indeed 'canonical' (Carandini & Heeger, 2012).

Although nonlinear, stimulus-dependent codes have been reported in many systems, the mechanisms underlying these phenomena are generally unclear. The mechanisms discussed include subthreshold activation, inhibitory inputs, modulation of the spiking threshold or the output nonlinearities (Assisi *et al.*, 2007; Schneider & Woolley, 2011; Massot *et al.*, 2012; Priebe & Ferster, 2012). Using a simplified model of the cricket auditory system (Fig. 6), we propose two candidate mechanisms that could underlie stimulus-dependent coding in this system: a logarithmic input nonlinearity with the crucial property of saturation (Fig. 7) and a broadly tuned feed-forward inhibition (Fig. 8) (Wu *et al.*, 2008; Poo & Isaacson, 2009; Liu *et al.*, 2011; Papadopoulou *et al.*, 2011; Carandini & Heeger, 2012).

The role of inhibition for adaptive spectral tuning and temporal selectivity

Modulation of inhibition is thought to induce adaptive and selective coding by changing the balance of excitation and inhibition in a stimulus-dependent manner (Wehr & Zador, 2003; Assisi *et al.*, 2007; Poo & Isaacson, 2009). In our network model, inhibition was mediated by ON1, which pooled activity of low-frequency and high-frequency receptors and was therefore broadly tuned (Fig. 3b). ON1 in the model altered the temporal selectivity of both ANs for multi-band stimuli (Fig. 8b). ON1 is usually associated with the enhancement of directional cues in the system (Horseman & Huber, 1994; Marsat & Pollack, 2005) but has also been shown to shape temporal selectivity in the cricket (Tunstall & Pollack, 2005). The role of ON1 suggested by our network model could be demonstrated by pharmacologically blocking its inhibitory synapses onto both ANs (without inhibition, temporal tuning should not change with stimulus condition) (Fig. 8b, green).

Although broad tuning of inhibition is a prerequisite for effective gain control (Fig. 7) (cf. Papadopoulou *et al.*, 2011; Carandini & Heeger, 2012), the timing of inhibition in the model controlled its specific effect on temporal coding (Fig. 9). Interestingly, the effect of inhibition from ON1 in the network model was similar to that observed in the barrel cortex of rodents; for AN2 in the model, it was coincident with nonpreferred stimuli and thereby more effective in their suppression (Fig. 9c) (cf. Wilent & Contreras, 2005). For AN1 in the model, it neutralised the excitation coming from nonpreferred high carrier frequencies (Fig. 9b).

A saturating nonlinearity as a peripheral transformation supporting stimulus-dependent codes

The network model revealed another transformation yielding stimulus-dependent coding, i.e. the saturating transformation in the periphery. This static nonlinearity produced broad receptor tuning for single-band stimuli and narrow receptor tuning for multi-band stimuli in the network model (Fig. 7d–g). Therefore, adaptive spectral tuning should be visible already in the population responses of auditory receptors as predicted by the network model, a surprising prediction that can be tested in future experiments.

Other studies have shown that gain control relies on accelerating output nonlinearities, such that the effective inhibitory drive is low for weak (single-band) stimuli and strong for strong (multi-band) stimuli (Rubin *et al.*, 2015). In our network model, there exist no accelerating output nonlinearities but only saturating input nonlinearities. Thus, the position of a nonlinearity (input or output) seems to determine what shape it needs to have to support gain control.

Our model is agnostic as to the biophysical underpinnings of this saturating nonlinearity in auditory receptors. Dendritic or firing rate nonlinearities are likely candidates (e.g. Jones & Gabbiani, 2012). Alternatively, nonlinearities could arise through nonlinear tympanal dynamics underlying mechanotransduction as demonstrated in other insect species, but not as yet for the cricket species studied here (Windmill *et al.*, 2005; Mhatre & Robert, 2013). Our study demonstrates the far-reaching and beneficial consequences of such nonlinearities. The contribution of tympanal nonlinearities could be tested using laser Doppler vibrometry (Mhatre & Robert, 2013).

Irrespective of its source [the nonlinearity's effect is general and does not depend on a specific functional form but works with any saturating input–output relation (see Fig. 7d–g)], every system with a compressive nonlinearity after a linear filter stage can exhibit adaptive coding [olfaction (Olsen *et al.*, 2010), vision/vertebrates (Sharpee *et al.*, 2006) and vision/insects (Jones & Gabbiani, 2012)]. For instance, the cochlea is known to exhibit a logarithmic input nonlinearity (Zilany *et al.*, 2009) and a standard filter-bank model also displays adaptive tuning (Fig. 7h). A cochlear logarithmic nonlinearity thus constitutes a peripheral mechanism that potentially contributes to the stimulus-dependent tuning observed in the primary auditory cortex (Gourévitch *et al.*, 2009).

Integration of peripheral nonlinearity and inhibition in complex neural networks

Although our simple network model was successful in reproducing suppression and decorrelation as observed in the experimental data, biological networks (including the cricket auditory system) are much more complex than our model and are equipped with a wealth of nonlinearities. How the mechanisms described here interact with a dynamic spiking threshold, spike-frequency adaptation, presynaptic inhibition or other sources of inhibition (Nolen & Hoy, 1987; Pollack, 1988; Wimmer *et al.*, 2008; Hildebrandt *et al.*, 2011) requires future attention. Dynamic changes in coding properties induced by feed-back gain control or spike-frequency adaptation support robust coding in the presence of a masker (e.g. background noise) (Rabinowitz *et al.*, 2013; Mesgarani *et al.*, 2014). These dynamic mechanisms are present in the cricket (Benda & Hennig, 2008) and could further enhance the robust and adaptive code explained by our static network model. Several studies have demonstrated that static nonlinearities in the periphery can contribute to nonlinear spectrotemporal tuning in mammalian auditory nerve fibers and in subcortical parts of the mammalian auditory system (Nelken *et al.*, 1997; Reiss *et al.*, 2007). Notably, two-tone or side-band suppression yield forms of nonlinear, stimulus-dependent tuning in the cricket and in mammalian auditory systems (Nolen & Hoy, 1987; Delgutte, 1990). However, most studies performed in mammalians measure response properties near threshold or consider the sound carrier as the relevant stimulus (and not the envelope), making a direct comparison with our results challenging (Carney & Yin, 1988; Kim & Young, 1994; Windmill *et al.*, 2005; Versteegh & van der Heijden, 2013). Also, it has been shown that bursts in AN2 support the separation of mating and predator signals (Marsat & Pollack, 2005). These and other nonlinear changes in a coding scheme can alleviate some of the trade-offs associated with sharpening tuning (Fig. 5) by enabling multiplexed, nonlinear encoding of two stimuli within a single spike train.

Note that the structure of the auditory system of crickets is shared among many species of crickets. However, despite a similar network layout, there exist considerable differences in the coding properties across species. The cricket *Teleogryllus oceanicus* differs from the species in this study (*Gryllus bimaculatus*) with regard to the input latencies for ON1 and the duration of filters in ON1 as well as the absolute information rates in AN1, AN2 and ON1 (Pollack, 1994; Marsat & Pollack, 2004, 2005). These differences could be the outcome of evolutionary adaptations to the different acoustic challenges faced by each species (cf. Tunstall & Pollack, 2005), e.g. the frequency spectra of the calling song differ between the species. It will thus be interesting to apply our approach to other species to establish the robustness of stimulus-dependent coding to variations in network parameters.

Conflict of interest

The authors have no conflicts of interest to declare.

Acknowledgements

This work was funded by grants from the Federal Ministry of Education and Research, Germany (01GQ1001A) and the Deutsche Forschungsgemeinschaft (SFB618, GK1589/1). We thank Jan Benda and Jan-Hendrik Schleimer for valuable discussions.

Abbreviations

AM, amplitude modulation; AN, ascending neuron; I/E, ratio ratio of total inhibitory and excitatory drive; LN, linear–nonlinear model; ON1, omega neuron 1; SPL, sound pressure level.

References

Aertsen, A.M. & Johannesma, P.I. (1981) The spectro-temporal receptive field. A functional characteristic of auditory neurons. *Biol. Cybern.*, **42**, 133–143.

Ahrens, M.B., Linden, J.F. & Sahani, M. (2008) Nonlinearities and contextual influences in auditory cortical responses modeled with multilinear spectrotemporal methods. *J. Neurosci.*, **28**, 1929–1942.

Assisi, C., Stopfer, M., Laurent, G. & Bazhenov, M. (2007) Adaptive regulation of sparseness by feedforward inhibition. *Nat. Neurosci.*, **10**, 1176–1184.

Atencio, C.A., Sharpee, T.O. & Schreiner, C.E. (2008) Cooperative nonlinearities in auditory cortical neurons. *Neuron*, **58**, 956–966.

Barlow, H. (2001) Redundancy reduction revisited. *Network*, **12**, 241–253.

Benda, J. & Hennig, M.R. (2008) Spike-frequency adaptation generates intensity invariance in a primary auditory interneuron. *J. Comput. Neurosci.*, **24**, 113–136.

Borst, A. & Theunissen, F.E. (1999) Information theory and neural coding. *Nat. Neurosci.*, **2**, 947–957.

Borst, A., Flanagin, V.L. & Sompolinsky, H. (2005) Adaptation without parameter change: dynamic gain control in motion detection. *Proc. Natl. Acad. Sci. USA*, **102**, 6172–6176.

Carandini, M. & Heeger, D.J. (2012) Normalization as a canonical neural computation. *Nat. Rev. Neurosci.*, **13**, 51–62.

Carney, L.H. & Yin, T.C. (1988) Temporal coding of resonances by low-frequency auditory nerve fibers: single-fiber responses and a population model. *J. Neurophysiol.*, **60**, 1653–1677.
Chacron, M.J., Doiron, B., Maler, L., Longtin, A. & Bastian, J. (2003) Non-classical receptive field mediates switch in a sensory neuron's frequency tuning. *Nature*, **423**, 77–81.
Chacron, M.J., Maler, L. & Bastian, J. (2005) Feedback and feedforward control of frequency tuning to naturalistic stimuli. *J. Neurosci.*, **25**, 5521–5532.
Clemens, J., Kutzki, O., Ronacher, B., Schreiber, S. & Wohlgemuth, S. (2011) Efficient transformation of an auditory population code in a small sensory system. *Proc. Natl. Acad. Sci. USA*, **108**, 13812–13817.
Clemens, J., Wohlgemuth, S. & Ronacher, B. (2012) Nonlinear computations underlying temporal and population sparseness in the auditory system of the grasshopper. *J. Neurosci.*, **32**, 10053–10062.
Delgutte, B. (1990) Two-tone rate suppression in auditory-nerve fibers: dependence on suppressor frequency and level. *Hearing Res.*, **49**, 225–246.
Faulkes, Z. & Pollack, G.S. (2000) Effects of inhibitory timing on contrast enhancement in auditory circuits in crickets (*Teleogryllus oceanicus*). *J. Neurophysiol.*, **84**, 1247–1255.
Faulkes, Z. & Pollack, G.S. (2001) Mechanisms of frequency-specific responses of omega neuron 1 in crickets (*Teleogryllus oceanicus*): a polysynaptic pathway for song? *J. Exp. Biol.*, **204**, 1295–1305.
Gawne, T.J. & Martin, J.M. (2002) Responses of primate visual cortical V4 neurons to simultaneously presented stimuli. *J. Neurophysiol.*, **88**, 1128–1135.
Gollisch, T., Schütze, H., Benda, J. & Herz, A.V.M. (2002) Energy integration describes sound-intensity coding in an insect auditory system. *J. Neurosci.*, **22**, 10434–10448.
Gourévitch, B., Noreña, A., Shaw, G. & Eggermont, J.J. (2009) Spectrotemporal receptive fields in anesthetized cat primary auditory cortex are context dependent. *Cereb. Cortex*, **19**, 1448–1461.
Hennig, M.R. (1988) Ascending auditory interneurons in the cricket *Teleogryllus commodus* (Walker): comparative physiology and direct connections with afferents. *J. Comp. Physiol. A.*, **163**, 135–143.
Hennig, M.R., Franz, A. & Stumpner, A. (2004) Processing of auditory information in insects. *Microsc. Res. Technol.*, **63**, 351–374.
Hildebrandt, K.J., Benda, J. & Hennig, R.M. (2011) Multiple arithmetic operations in a single neuron: the recruitment of adaptation processes in the cricket auditory pathway depends on sensory context. *J. Neurosci.*, **31**, 14142–14150.
Hirtz, R. & Wiese, K. (1997) Ultrastructure of synaptic contacts between identified neurons of the auditory pathway in *Gryllus bimaculatus* DeGeer. *J. Comp. Neurol.*, **386**, 347–357.
Horseman, G. & Huber, F. (1994) Sound localisation in crickets. I. Contralateral inhibition of an ascending auditory interneuron (AN1) in the cricket *Gryllus bimaculatus*. *J. Comp. Physiol. A.*, **175**, 389–398.
Imaizumi, K. & Pollack, G.S. (1999) Neural coding of sound frequency by cricket auditory receptors. *J. Neurosci.*, **19**, 1508–1516.
Imaizumi, K. & Pollack, G.S. (2001) Neural representation of sound amplitude by functionally different auditory receptors in crickets. *J. Acoust. Soc. Am.*, **109**, 1247–1260.
Jones, P.W. & Gabbiani, F. (2012) Logarithmic compression of sensory signals within the dendritic tree of a collision-sensitive neuron. *J. Neurosci.*, **32**, 4923–4934.
Kim, P.J. & Young, E.D. (1994) Comparative analysis of spectro-temporal receptive fields, reverse correlation functions, and frequency tuning curves of auditory-nerve fibers. *J. Acoust. Soc. Am.*, **95**, 410–422.
Libersat, F., Murray, J.A. & Hoy, R. (1994) Frequency as a releaser in the courtship song of two crickets, *Gryllus bimaculatus* (de Geer) and *Teleogryllus oceanicus*: a neuroethological analysis. *J. Comp. Physiol. A.*, **174**, 485–494.
Linden, J.F., Liu, R.C., Sahani, M., Schreiner, C.E. & Merzenich, M.M. (2003) Spectrotemporal structure of receptive fields in areas AI and AAF of mouse auditory cortex. *J. Neurophysiol.*, **90**, 2660–2675.
Liu, B.-H., Li, Y.-T., Ma, W.-P., Pan, C.-J., Zhang, L.I. & Tao, H.W. (2011) Broad inhibition sharpens orientation selectivity by expanding input dynamic range in mouse simple cells. *Neuron*, **71**, 542–554.
Machens, C.K., Wehr, M. & Zador, A.M. (2004) Linearity of cortical receptive fields measured with natural sounds. *J. Neurosci.*, **24**, 1089–1100.
Margoliash, D. & Konishi, M. (1985) Auditory representation of autogenous song in the song system of white-crowned sparrows. *Proc. Natl. Acad. Sci. USA*, **82**, 5997–6000.
Marsat, G. & Pollack, G.S. (2004) Differential temporal coding of rhythmically diverse acoustic signals by a single interneuron. *J. Neurophysiol.*, **92**, 939–948.
Marsat, G. & Pollack, G.S. (2005) Effect of the temporal pattern of contralateral inhibition on sound localization cues. *J. Neurosci.*, **25**, 6137–6144.
Marsat, G. & Pollack, G.S. (2006) A behavioral role for feature detection by sensory bursts. *J. Neurosci.*, **26**, 10542–10547.
Massot, C., Schneider, A.D., Chacron, M.J. & Cullen, K.E. (2012) The vestibular system implements a linear–nonlinear transformation in order to encode self-motion. *PLoS Biol.*, **10**, e1001365.
Mesgarani, N., David, S.V., Fritz, J.B. & Shamma, S.A. (2014) Mechanisms of noise robust representation of speech in primary auditory cortex. *Proc. Natl. Acad. Sci. USA*, **111**, 6792–6797.
Mhatre, N. & Robert, D. (2013) A tympanal insect ear exploits a critical oscillator for active amplification and tuning. *Curr. Biol.*, **23**, 1952–1957.
Middleton, J.W., Omar, C., Doiron, B. & Simons, D.J. (2012) Neural correlation is stimulus modulated by feedforward inhibitory circuitry. *J. Neurosci.*, **32**, 506–518.
Narayan, R., Best, V., Ozmeral, E., Mcclaine, E., Dent, M., Cunningham, B.S. & Sen, K. (2007) Cortical interference effects in the cocktail party problem. *Nat. Neurosci.*, **10**, 1601–1607.
Nelken, I., Kim, P.J. & Young, E.D. (1997) Linear and nonlinear spectral integration in Type IV neurons of the dorsal cochlear nucleus. II. Predicting responses with the use of nonlinear models. *J. Neurophysiol.*, **78**, 800–811.
Nolen, T.G. & Hoy, R. (1984) Initiation of behavior by single neurons: the role of behavioral context. *Science*, **226**, 992–994.
Nolen, T.G. & Hoy, R. (1987) Postsynaptic inhibition mediates high-frequency selectivity in the cricket *Teleogryllus oceanicus*: implications for flight phonotaxis behavior. *J. Neurosci.*, **7**, 2081–2096.
Olsen, S.R., Bhandawat, V. & Wilson, R.I. (2010) Divisive normalization in olfactory population codes. *Neuron*, **66**, 287–299.
Papadopoulou, M., Cassenaer, S., Nowotny, T. & Laurent, G. (2011) Normalization for sparse encoding of odors by a wide-field interneuron. *Science*, **332**, 721–725.
Pollack, G.S. (1988) Selective attention in an insect auditory neuron. *J. Neurosci.*, **8**, 2635–2639.
Pollack, G.S. (1994) Synaptic inputs to the omega neuron of the cricket *Teleogryllus oceanicus*: differences in EPSP waveforms evoke by low and high sound frequencies. *J. Comp. Physiol. A.*, **174**, 83–89.
Pollack, G.S. & Imaizumi, K. (1999) Neural analysis of sound frequency in insects. *BioEssays*, **21**, 295–303.
Poo, C. & Isaacson, J.S. (2009) Odor representations in olfactory cortex: 'sparse' coding, global inhibition, and oscillations. *Neuron*, **62**, 850–861.
Popov, A.V. & Shuvalov, V.F. (1977) Phonotactic behavior of crickets. *J. Comp. Physiol. A.*, **119**, 111–126.
Pouget, A., Deneve, S., Ducom, J.C. & Latham, P.E. (1999) Narrow versus wide tuning curves: what's best for a population code? *Neural Comput.*, **11**, 85–90.
Priebe, N.J. & Ferster, D. (2012) Mechanisms of neuronal computation in mammalian visual cortex. *Neuron*, **75**, 194–208.
Rabinowitz, N.C., Willmore, B.D.B., King, A.J. & Schnupp, J.W.H. (2013) Constructing noise-invariant representations of sound in the auditory pathway. *PLoS Biol.*, **11**, e1001710.
Reiss, L.A., Bandyopadhyay, S. & Young, E.D. (2007) Effects of stimulus spectral contrast on receptive fields of dorsal cochlear nucleus neurons. *J. Neurophysiol.*, **98**, 2133–2143.
Rubin, D.B., Van Hooser, S.D. & Miller, K.D. (2015) The Stabilized Supralinear Network: a unifying circuit motif underlying multi-input integration in sensory cortex. *Neuron*, **85**, 402–417.
Schneider, D.M. & Woolley, S.M. (2011) Extra-classical tuning predicts stimulus-dependent receptive fields in auditory neurons. *J. Neurosci.*, **31**, 11867–11878.
Schwartz, O., Pillow, J.W., Rust, N.C. & Simoncelli, E.P. (2006) Spike-triggered neural characterization. *J. Vision*, **6**, 484–507.
Selverston, A.I., Kleindienst, H. & Huber, F. (1985) Synaptic connectivity between cricket auditory interneurons as studied by selective photoinactivation. *J. Neurosci.*, **5**, 1283–1292.
Seriès, P., Latham, P.E. & Pouget, A. (2004) Tuning curve sharpening for orientation selectivity: coding efficiency and the impact of correlations. *Nat. Neurosci.*, **7**, 1129–1135.
Sharpee, T.O., Sugihara, H., Kurgansky, A.V., Rebrik, S.P., Stryker, M.P. & Miller, K.D. (2006) Adaptive filtering enhances information transmission in visual cortex. *Nature*, **439**, 936–942.
Sobel, E.C. & Tank, D.W. (1994) *In vivo* Ca^{2+} dynamics in a cricket auditory neuron: an example of chemical computation. *Science*, **263**, 823–826.
Tunstall, D.N. & Pollack, G.S. (2005) Temporal and directional processing by an identified interneuron, ON1, compared in cricket species that sing with different tempos. *J. Comp. Physiol. A.*, **191**, 363–372.
Versteegh, C.P.C. & van der Heijden, M. (2013) The spatial buildup of compression and suppression in the mammalian cochlea. *JARO*, **14**, 523–545.

Vinje, W.E. & Gallant, J.L. (2000) Sparse coding and decorrelation in primary visual cortex during natural vision. *Science*, **287**, 1273–1276.

Wehr, M. & Zador, A.M. (2003) Balanced inhibition underlies tuning and sharpens spike timing in auditory cortex. *Nature*, **426**, 442–446.

Wilent, W.B. & Contreras, D. (2005) Dynamics of excitation and inhibition underlying stimulus selectivity in rat somatosensory cortex. *Nat. Neurosci.*, **8**, 1364–1370.

Wimmer, K., Hildebrandt, J.K., Hennig, M.R. & Obermayer, K. (2008) Adaptation and selective information transmission in the cricket auditory neuron AN2. *PLoS Comput. Biol.*, **4**, e1000182.

Windmill, J.F.C., Göpfert, M.C. & Robert, D. (2005) Tympanal travelling waves in migratory locusts. *J. Exp. Biol.*, **208**, 157–168.

Wohlers, D.W. & Huber, F. (1982) Processing of sound signals by six types of neurons in the prothoracic ganglion of the cricket, *Gryllus campestris* L. *J. Comp. Physiol. A.*, **146**, 161–173.

Wu, G.K., Arbuckle, R., Liu, B.-H., Tao, H.W. & Zhang, L.I. (2008) Lateral sharpening of cortical frequency tuning by approximately balanced inhibition. *Neuron*, **58**, 132–143.

Wyttenbach, R.A., May, M.L. & Hoy, R. (1996) Categorical perception of sound frequency by crickets. *Science*, **273**, 1542–1544.

Zhang, K. & Sejnowski, T.J. (1999) Neuronal tuning: to sharpen or broaden? *Neural Comput.*, **11**, 75–84.

Ziehm, R. (2014) Intensity adaptation in the cricket auditory system, PhD thesis, Humboldt-Universität zu Berlin.

Zilany, M.S.A., Bruce, I.C., Nelson, P.C. & Carney, L.H. (2009) A phenomenological model of the synapse between the inner hair cell and auditory nerve: long-term adaptation with power-law dynamics. *J. Acoust. Soc. Am.*, **126**, 2390–2412.

Zoccolan, D., Cox, D.D. & Dicarlo, J.J. (2005) Multiple object response normalization in monkey inferotemporal cortex. *J. Neurosci.*, **25**, 8150–8164.